

INELASTIC ELECTRON SCATTERING  
IN  $^{28}\text{Si}$  BETWEEN 4 MEV AND  
50 MEV EXCITATION ENERGY

Edward Echerd Hunter



# NAVAL POSTGRADUATE SCHOOL

## Monterey, California



# THESIS

INELASTIC ELECTRON SCATTERING  
IN  $^{28}\text{Si}$  BETWEEN 4 MeV AND  
50 MeV EXCITATION ENERGY

by

Edward Echerd Hunter

and

Gregory Pozinsky

June 1978

Thesis Co-Advisors:

F.R. Buskirk  
R. Pitthan

Approved for public release; distribution unlimited.

T18407



UNCLASSIFIED

SECURITY CLASSIFICATION OF THIS PAGE (When Data Entered)

REPORT DOCUMENTATION PAGE		READ INSTRUCTIONS BEFORE COMPLETING FORM
1. REPORT NUMBER	2. GOVT ACCESSION NO.	3. RECIPIENT'S CATALOG NUMBER
4. TITLE (and Subtitle) Inelastic Electron Scattering in $^{28}\text{Si}$ Between 4 MeV and 50 MeV Excitation Energy		5. TYPE OF REPORT & PERIOD COVERED Master's Thesis; June 1978
7. AUTHOR(s) Edward Echerd Hunter Gregory Pozinsky		6. PERFORMING ORG. REPORT NUMBER
9. PERFORMING ORGANIZATION NAME AND ADDRESS Naval Postgraduate School Monterey, California 93940		8. CONTRACT OR GRANT NUMBER(s)
11. CONTROLLING OFFICE NAME AND ADDRESS Naval Postgraduate School Monterey, California 93940		10. PROGRAM ELEMENT, PROJECT, TASK AREA & WORK UNIT NUMBERS
14. MONITORING AGENCY NAME & ADDRESS (if different from Controlling Office)		12. REPORT DATE June 1978
		13. NUMBER OF PAGES 62
		15. SECURITY CLASS. (of this report) Unclassified
		15a. DECLASSIFICATION/DOWNGRADING SCHEDULE
16. DISTRIBUTION STATEMENT (of this Report)  Approved for public release; distribution unlimited.		
17. DISTRIBUTION STATEMENT (of the abstract entered in Block 20, if different from Report)		
18. SUPPLEMENTARY NOTES		
19. KEY WORDS (Continue on reverse side if necessary and identify by block number)  $^{28}\text{Si}$ Inelastic Electron Scattering		
20. ABSTRACT (Continue on reverse side if necessary and identify by block number) 91.2 MeV electrons were used to study $^{28}\text{Si}$ in the excitation range from 4 to 50 MeV. Fragmentation of E2 strength into states below the GQR region was found, with states between 0 and 15 MeV exhausting 35% of the E2 isoscalar EWSR. Available ( $\gamma$ ,abs) data were used to disentangle E1 and E2 strength in the region 15 to 30 MeV and show E2 strength separated into two distinct groups in		



## (20. ABSTRACT Continued)

this region. A cluster of E2 strength centered at 17.5 MeV and believed to be in the oblate ground state well exhausts 22% of the E2 isoscalar EWSR and a broad but clearly separate group of strength from 20 to 30 MeV exhausts 65% of the E2 isovector EWSR. Significant transition strength was found between 30 and 50 MeV which exhausts between 25 and 35% of the total E2 EWSR. Evidence was found for the existence of an E2 giant resonance corresponding to the oblate well of  $^{28}\text{Si}$  at 24 MeV.



Approved for public release; distribution unlimited.

Inelastic Electron Scattering  
in  $^{28}\text{Si}$  Between 4 MeV and  
50 MeV Excitation Energy

by

Edward Echerd Hunter  
Lieutenant, United States Navy  
B.S., North Carolina State University, 1969

and

Gregory Pozinsky  
Lieutenant, United States Navy  
B.S., United States Naval Academy, 1973

Submitted in partial fulfillment of the  
requirements for the degree of

MASTER OF SCIENCE IN PHYSICS

from the

NAVAL POSTGRADUATE SCHOOL

June 1978



## ABSTRACT

91.2 MeV electrons were used to study  $^{28}\text{Si}$  in the excitation range from 4 to 50 MeV. Fragmentation of E2 strength into states below the GQR region was found, with states between 0 and 15 MeV exhausting 35% of the E2 isoscalar EWSR. Available  $(\gamma, \text{abs})$  data were used to disentangle E1 and E2 strength in the region 15 to 30 MeV and show E2 strength separated into two distinct groups in this region. A cluster of E2 strength centered at 17.5 MeV and believed to be in the oblate ground state well exhausts 22% of the E2 isoscalar EWSR and a broad but clearly separate group of strength from 20 to 30 MeV exhausts 65% of the E2 isovector EWSR. Significant transition strength was found between 30 and 50 MeV which exhausts between 25 and 35% of the total E2 EWSR. Evidence was found for the existence of an E2 giant resonance corresponding to the oblate well of  $^{28}\text{Si}$  at 24 MeV.



## TABLE OF CONTENTS

I.	INTRODUCTION -----	10
II.	EXPERIMENTAL DETAILS -----	11
III.	THEORY -----	12
	A. ELECTRON SCATTERING -----	12
	B. NUCLEAR MODELS -----	15
IV.	DATA ANALYSIS -----	18
	A. DATA COLLECTION -----	18
	B. BACKGROUND -----	18
	C. LINE FITTING -----	19
	D. SUM RULES -----	20
	E. PHOTONUCLEAR DATA -----	21
V.	RESULTS -----	24
VI.	CONCLUSIONS -----	31
	LIST OF REFERENCES -----	60
	INITIAL DISTRIBUTION LIST -----	62



## LIST OF TABLES

I.	Experimental parameters, inelastic electron scattering from $^{28}\text{Si}$ -----	32
II.	Parameters for conversion of photon absorbtion cross section to equivalent electron scattering cross section -----	33
III.	Summary of results, 4 to 15 MeV -----	34
IV.	Distribution of E2 strength 0 to 50 MeV -----	35
V.	Contribution of E2 strength to $\gamma$ cross section --	36



# LIST OF FIGURES

1.	Inelastic spectrum, 105°, 120° -----	41
2.	Inelastic spectrum, 105°, 120° -----	42
3.	Comparison of DWBA cross sections -----	43
4.	Comparison of Goldhaber-Teller, Steinwedel-Jensen, and Myers-Swiatecki models for DWBA calculations for El transitions -----	44
5.	Gamma absorbtion data from Ahrens, et al. (Ahrens 75) -----	45
6.	Comparison of the DWBA and experimental form factors for the state at 5.1 MeV -----	46
7.	Comparison of the DWBA and experimental form factors for the state at 7.0 MeV -----	47
8.	Comparison of the DWBA and experimental form factors for the state at 9.9 MeV -----	48
9.	Comparison of the DWBA and experimental form factors for the state at 11.2 MeV -----	49
10.	Comparison of the DWBA and experimental form factors for the state at 13.0 MeV -----	50
11.	Comparison of the DWBA and experimental form factors for the state(s) at 15 MeV. The (γ,abs) cross section strength has been subtracted -----	51
12.	Comparison of the DWBA and experimental form factors for the region 15 to 20 MeV with the (γ,abs) strength subtracted -----	52
13.	Comparison of the DWBA and experimental form factors for the region 20 to 30 MeV. The (γ,abs) cross section strength has been subtracted -----	53
14.	Inelastic cross section at 60°, 12 to 30 MeV, showing the subtraction of (γ,abs) data -----	54
15.	Inelastic cross section at 75°, 12 to 30 MeV, showing the subtraction of (γ,abs) data -----	55



16.	Inelastic cross section at $90^\circ$ , 12 to 30 MeV, showing the subtraction of ( $\gamma$ ,abs) data -----	56
17.	Inelastic cross section at $105^\circ$ , 12 to 30 MeV, showing the subtraction of ( $\gamma$ ,abs) data -----	57
18.	Inelastic cross section at $120^\circ$ , 12 to 30 MeV, showing the subtraction of ( $\gamma$ ,abs) data -----	58
19.	Inelastic cross section at $120^\circ$ , 12 to 30 MeV, showing the maximum background -----	59



## ACKNOWLEDGMENTS

We would like to express our thanks and appreciation to our Thesis Advisors, Professors Fred R. Buskirk and W. Rainer Pitthan for their many long hours of competent and eager instruction, advice, and assistance. Professor Pitthan's guidance in utilizing the various computer programs for data reduction and analysis was invaluable in the completion of this work. Professor Buskirk's advice during the theoretical portion of this thesis was invaluable as well as his many long hours repairing, running, and improving the performance of the LINAC during the data acquisition phase.

Thanks also to Professor John N. Dyer for his helpful classnotes, class room instruction, and assistance in operating the LINAC.

We thank Mr. H. (Mac) McFarland and Mr. D. Snyder for their invaluable technical skills, and hard work in keeping the LINAC operational.

We are indebted to the operational staff of the W.R. Church Computer Center for their assistance in processing our computer programs.

Thanks, also, to our fellow students, LCDR Hubert Hass, FGN, and LT Daniel Meyer, USN, for their cooperation in our joint data taking and for their friendly competition.

Finally, we would like to thank our wives, Linda and Ruth Ann for their patience and encouragement during the course of our postgraduate studies.



## I. INTRODUCTION

In light nuclei,  $A < 28$ , the location of a giant quadrupole resonance (GQR) has not been as clearly established as in heavier nuclei. However, recent  $\alpha$ -scattering experiments have revealed the existence of an E2 strength of 30% - 60% of the energy weighted sum rule (EWSR) for isoscalar quadrupole excitations between 12 and 32 MeV (YouR 77). Unlike heavier nuclei, the GQR strength is not concentrated in a single peak but spread over several states or fragmented among many states over a wide energy range. Similarly, total photon absorption measurements have shown that the dipole strength is distributed from 15 to 30 MeV for light nuclei. As a consequence, giant dipole (E1,GDR) and quadrupole (E2,GDR) strength is not as easily separated as in heavier nuclei, where they can be separated by a line shape fit.

In this paper we will investigate giant multipole resonances and bound states in  $^{28}\text{Si}$  through inelastic scattering of electrons with 92 MeV incident energy.



## II. EXPERIMENTAL DETAILS

Data were collected using the 120 MeV Naval Postgraduate School Linear Accelerator. The target was self supporting  $^{28}\text{Si}$  of semi-conductor quality obtained from Fairchild Industries. Scattering angles were  $60^\circ$ ,  $75^\circ$ ,  $90^\circ$ ,  $105^\circ$ , and  $120^\circ$  and transmission geometry was used throughout. Details concerning the operation and characteristics of the NPS LINAC can be found in Pitthan, et al. (Pit 77).

The 16 inch spectrometer does not have an open back and therefore produces an appreciable ghost peak. Measurements on  $^{12}\text{C}$  have shown that the ghost peak appears at 92% of the energy of the elastic peak and has a nominal half-width of approximately 4.5 MeV. This correction was included in the analysis of all runs and adds significantly to the uncertainty in evaluation of data in the 4-8 MeV region of the spectra.

The counting system consists of a ten-counter ladder in the focal plane of the spectrometer with two backing counters forming 10 triple coincidence channels. The average beam current was controlled to give count rates lower than 20 counts per second and a subsequent accidental coincidence rate of less than 5%.



### III. THEORY

#### A. ELECTRON SCATTERING

The theory of elastic and inelastic scattering from nuclei has been documented in detail by Überall (Übe 71). Beginning with the Mott cross section for scattering of a relativistic electron from a spinless, point nucleus, the differential elastic cross section can be expressed as

$$\left(\frac{d\sigma}{d\Omega}\right)_{el} = \left(\frac{d\sigma}{d\Omega}\right)_{Mott} |F(q)|^2 R ,$$

where

$$\left(\frac{d\sigma}{d\Omega}\right)_{Mott} = \left(\frac{ze^2}{2Ei}\right)^2 \frac{\cos^2 \theta/2}{\sin^4 \theta/2}$$

$$F(q) = \int e^{-i\vec{q} \cdot \vec{r}} \rho(r) d^3r$$

$R$  = recoil correction factor

$\vec{q}$  = momentum transfer

$\rho(r)$  = nuclear charge density.

The inelastic cross section is much more complex and consists of separate terms for electric and magnetic transitions, as well as transverse and longitudinal components representing decomposition of the electromagnetic



electron-nuclear interaction into components parallel and perpendicular to the three-vector momentum transfer  $\vec{q}$ .

Following Theissen (The 72), the plane wave Born approximation (PWBA) for the differential inelastic cross section can be expressed as a sum over the electric (e) and magnetic (m) multipole transitions:

$$\left(\frac{d\sigma}{d\Omega}\right)_{\text{DWBA}} = \sum_{\lambda} \left(\frac{d\sigma}{d\Omega}\right)_{e,\lambda} + \sum_{\lambda} \left(\frac{d\sigma}{d\Omega}\right)_{m,\lambda}.$$

The expanded forms are as follows:

$$\begin{aligned} \left(\frac{d\sigma}{d\Omega}\right)_{e,\lambda} &= \alpha^2 a_{\lambda} q^{2\lambda} K_O^{-2} [\lambda(\lambda+1)^{-1} B(c\lambda, q, I_O \rightarrow I_n) V_L(\theta) \\ &\quad + B(E\lambda, q, I_O \rightarrow I_x) V_T(\theta)] R; \end{aligned}$$

$$\left(\frac{d\sigma}{d\Omega}\right)_{m,\lambda} = \alpha^2 a_{\lambda} q^{2\lambda} K_O^{-2} B(M\lambda, q, I_O \rightarrow I_x) V_T(\theta) R.$$

In these equations:

$$a_{\lambda} = 4\pi\lambda^{-1}(\lambda+1)[(2\lambda+1)!!]^{-2}$$

$$K_O = E_O/\hbar c$$

$$R = [1 + \hbar c(K_O/Mc^2)(1 - \cos \theta)]^{-1}$$

$$\lambda = \text{transition multipolarity}$$

$$\alpha = \text{fine structure constant}$$

$$E_O = \text{primary electron energy}$$



$\theta$  = scattering angle

$M$  = nuclear mass

The terms  $V_L(\theta)$  and  $V_T(\theta)$  represent the decomposition parallel and perpendicular to the momentum transfer three vector  $\vec{q}$  and are expressed as follows:

$$V_L(\theta) = \frac{1}{2} \frac{(1 + \cos \theta)}{(y - \cos \theta)^2}$$

$$V_T(\theta) = \frac{1}{4} \frac{(2y + 1 - \cos \theta)}{(y - \cos \theta)(1 + \cos \theta)}$$

$$y = \frac{1 + E_x^2}{2E_O(E_O - E_x)}$$

The plane wave Born approximation is accurate for light nuclei ( $\alpha Z \ll 1$ ) but deteriorates in accuracy for nuclei with higher  $Z$  ( $\alpha Z \gtrsim 1$ ), when the plane wave representation of the incident electrons is distorted by the Coulomb field of the nucleus. A more accurate distorted wave Born approximation (DWBA) can be obtained by solving the Dirac equation for the electron with numerical integration (TuaW 68). The distorted wave calculations are made for  $\lambda = 1, 2, 3 \dots$  with the cross section normalized to reduced matrix elements  $B(\lambda, q, I_O \rightarrow I_x) = 1 \text{ e}^2 \text{ fm}^{2\lambda}$ .

Inelastic cross sections can be determined relative to the elastic cross section by the formula



$$\frac{d\sigma_I}{d\Omega} = \frac{A_I}{A_E} \frac{d\sigma_E}{d\Omega} ,$$

where  $A_I$  and  $A_E$  designate the areas under inelastic and elastic curves. The use of the relative cross section  $\frac{d\sigma_I}{d\Omega}$ , which in this case of plane wave Born approximations is identical with the form factor squared,  $F^2(q)$ , allows a convenient representation of data because the use of  $\sigma_{\text{Mott}}$  takes out most of the trivial dependence on scattering parameters and emphasizes the effects of nuclear structure (ZieP 68).  $B(E\lambda)$  values can be extracted from the  $\sigma_I/\sigma_{\text{Mott}}$  experimental values by comparison to the computer calculated values for each angle. The multipolarity of the transition can be similarly determined.

## B. NUCLEAR MODELS

Giant resonances in nuclei can be understood to a great extent on the basis of macroscopic collective models of nuclear excitation. Goldhaber and Teller proposed three such macroscopic models as follows (GolT 48):

(1) Elastic binding of neutrons and protons resulting in resonances with excitation energy independent of mass number  $A$ .

(2) Density and vibrations of neutrons and protons, each inside a fixed surface, against each other. This model yields an  $A^{-1/3}$  proportionality relationship for resonance energies and was further expanded by Steinwedel and Jensen (SteJ 50).



(3) Vibrations of interpenetrating density distributions of neutrons and protons with a resonant energy proportional to  $A^{-1/6}$  (GT model).

Überall generalized the GT model by combining the interactions of protons, with spin up or down with neutrons, with spin up or down, resulting in four types of resonate modes (Übe 71):

- (1)  $(P\uparrow, P\downarrow)$  against  $(n\uparrow, n\downarrow)$ . The isospin or original GT mode.
- (2)  $(P\uparrow, n\uparrow)$  against  $(P\downarrow, n\downarrow)$ . The spin-wave mode.
- (3)  $(P\uparrow, n\downarrow)$  against  $(P\downarrow, n\uparrow)$ . The spin-isospin mode.
- (4) A mode with all four "fluids" oscillating in phase. This type of interaction would give rise to a "breathing" or monopole resonance.

Goldhaber and Teller, in their third proposed model, assumed a rigid displacement of the ground state charge distribution which gives the relation

$$\rho(r) \approx \rho_0(r) - \frac{1}{2} \vec{d} \cdot \nabla \rho_0(r) ,$$

where  $\vec{d}$  is the displacement vector between the proton and neutron mass centers and is small. This distribution is applicable to dipole transitions but can be generalized to other multipoles by assuming that the ground state density  $\rho_0(r)$  is deformed by a scale factor (Übe 71)

$$\rho(r) = \rho_0(r) - \eta r [d\rho_0(r)/dr]^{\ell}$$



Steinwedel and Jensen (SteJ 50) have proposed a model (SJ model) which describes collective vibrations of neutrons and protons in terms of changes in the relative densities of the two fluids inside a rigid surface. Model 2 of Goldhaber and Teller requires that

$$\rho(r) = \rho_p(r) + \rho_n(r) = \text{constant}$$

and leads to the relationship

$$E_1 \approx 80 A^{-1/3}$$

for the giant dipole resonance energy.

Myers and Swiatecki (MyS 77) have proposed a model (MS model) which is a combination of the GT and SJ modes. Relative magnitudes are determined mainly by GT and SJ coupling and their associated forces and inertias, although the MS model is mainly a GT mode with a mixture of the SJ mode increasing for heavier nuclei. Myers and Swiatecki also found a dependence on A for resonance energy which is somewhere between that of the GT and SJ modes. A comparison of the DWBA form factor for E1 between GT, SJ, and MS models can be seen in Figure 4.



#### IV. DATA ANALYSIS

##### A. DATA COLLECTION

Data were collected for each angle over the range 93.5 - 85.5 MeV scattered electron energy for the elastic scattering and 88 - 40 MeV for inelastic scattering. All runs were made in 0.1 MeV steps. Total counts for each step were determined by integration of the beam current to preset values.

Data from the counting system were recorded on a teletype machine and on a seven-track magnetic tape compatible with the IBM 360/67 Computer System.

##### B. BACKGROUND

Three types of background have to be considered:

(1) "Target out" background which is low due to the triple coincidence set up of the counting ladder and which is fairly constant over time.

(2) "Target in" background caused by scattering of electrons from the target and subsequently off the spectrometer wall into the counting system.

(3) The radiation tail caused by photon emission (1) during, (2) before or after, and (3) Møller scattering. The Born approximation radiation tail is described in detail by Isabelle and Bishop (IsaB 63). Modifications which account for deviations from the Born approximation are described in



Buskirk and Pitthan (BusP 76) and are incorporated as a portion of the line shape fitting computer program.

The overall background was expressed as a function of the excitation energy by the following formula:

$$\text{BGR}(E_f) = P_1 + \frac{P_2}{E_f} + \text{RT}(E_f) .$$

This function was incorporated in the line fitting program with  $P_1$  and  $P_2$  the fitted parameters.

### C. LINE FITTING

The data for each run were fit using the line shape fitting routine of Pitthan (Pit 73). Most resonances were fit using a Breit-Wigner line shape for the B-value distribution:

$$\frac{dB}{dE_x} = \left| \frac{dB}{dE_x} \right|_{\text{max}} \frac{(\Gamma/2)^2}{(E_x - E_0)^2 + (\Gamma/2)^2}$$

as described in Gordon and Pitthan (GorP 77). Resonance lines with half-widths on the order of the elastic peak were considered to have their line shape determined by the elastic peak and hence were fit with a Gaussian line shape.

The parameters  $E_x$ ,  $\Gamma$ , and the elastic to inelastic peakheight ratios were fitted for each resonance. The fitting program varies these parameters to give a minimum chi-squared ( $\chi^2$ ) value. The value of  $\chi^2$  is defined as:



$$\chi^2 = \sum_n (x_i - x_o)^2 / \sigma^2$$

$x_i$  = calculated value of cross section

$x_o$  = measured value of cross section

$\sigma$  = standard deviation associated with  $x_i$

As described by Pitthan et al. (Pit 77), the total  $\chi^2$  is related to the number of degrees of freedom in the total fit. The number of degrees of freedom is defined as the number of experimental points (~400) less the number of parameters used for the fit (3 for each line fit and 2 for the background). For a good fit, the theoretical value of  $\chi^2$  per degree of freedom should approach  $\chi^2 = 1$ . The myriad structure evidenced in our data made line fitting particularly difficult and the actual value was considered less important than attempting a realistic as well as accurate representation of the experimental data and establishing a credible background.

#### D. SUM RULES

In addition to the reduced transition probability or B-value, a measure of transition strength is a percentage of the sum rule strength. The following formulas were used in this work for the calculation of sum rules:



$$S(E\lambda, \lambda > 1) = E_x \cdot B(E\lambda) = \frac{Z\lambda(2\lambda+1)^2 \hbar^2}{8\pi M_P} \langle R^{2\lambda-2} \rangle \quad (\text{WarW 69})$$

$$S(E1) = E_x \cdot B(E1) = \frac{9\hbar^2}{8\pi M_P} \frac{NZ}{A}$$

$$S(E0) = E_x \cdot |M_{fi}|^2 = \frac{\hbar^2}{M_P} A \cdot \langle R^2 \rangle \quad (\text{Fer 57})$$

## E. PHOTONUCLEAR DATA

The Giant Dipole Resonance has been studied using the gamma absorption ( $\gamma$ ,abs) technique. The cross sections determined using ( $\gamma$ ,abs) measure mainly dipole (E1) strength, and by subtracting the ( $\gamma$ ,abs) data from our results, contributions from higher multipole transitions can be determined.

The total cross section measured from ( $\gamma$ ,abs) is related to B-values by the formula

$$\int \sigma_\gamma dE_\gamma = 8\pi^3 \hbar c \alpha \frac{\lambda+1}{\lambda} \frac{1}{[(2\lambda+1)!!]^2} k^{2\lambda-1} B(E\lambda, k)$$

where

$$k = E_x / \hbar c$$

$$\lambda = \text{multipolarity}$$

$$\alpha = \text{fine structure constant}$$

(Pit 77).



The ( $\gamma$ ,abs) data from Ahrens et al. (Ahrens 75) were read from the graph in Figure 5. The data were then related to our (e,e') data using the following procedure:

(1) The formula for

$$\int \sigma_{\gamma} dE_{\gamma} \quad \text{gives} \quad \frac{d\sigma_{\gamma}}{dE_{\gamma}} = 4.02B(E1,k) \quad \text{for} \quad \lambda = 1 .$$

(2) This function was used to convert  $d\sigma/dE_x$  values to  $\frac{d^2\sigma}{dE d\Omega}$  compatible with our data. Values of  $\frac{d\sigma}{d\Omega}$  were computed for  $B(E1) = 1 \text{ fm}^2$  using the DWBA program of Tuan, et al. (TuaW 68) using the Myers-Swiatecki model. The computed values were fit with a three parameter parabolic function to give

$$\frac{d\sigma}{d\Omega} (\theta, E_x \text{ } B(E1) = 1 \text{ fm}^2) = P_1 + P_2(E_x) + P_3(E_x)^2$$

The calculated parameters are listed in Table II.

(3) The values of  $\frac{d^2\sigma}{dE_x d\Omega}$  were calculated as

$$\frac{d^2\sigma}{dE_x d\Omega} = \frac{d\sigma_x}{dE_x} \cdot \frac{d\sigma}{d\Omega} .$$

These values were calculated for each of our five runs.

(4) The converted ( $\gamma$ ,abs) data represent the equivalent total (e,e') E1 transition cross section in the region 10 to 30 MeV. By subtracting this data from our data, which represents the total  $E\lambda$  cross section, the  $E\lambda$ ,  $\lambda > 1$  cross



section can be represented. This analysis was carried out for each of our spectra.



## V. RESULTS

A. The line shape fit program was used to analyze the resolved states (or group of states) in the region 4 to 15 MeV. Such states were found at 5.1, 7.0, 9.9, 11.2, 13.0, and 15.0 MeV. With the exception of the state at 7.0 MeV these states were all found to be predominantly of E2 character, exhausting 2.4, 3.5, 3.7, 6.6, and 7% of the E2 isoscalar EWSR respectively. The state at 7.0 MeV was determined to be E3 in character and exhausts 22% of the E3 isoscalar EWSR. Results are summarized in Table III and Figures 6 to 11. The state found at 15 MeV had to be treated differently than the other states. The  $(\gamma, \text{abs})$  data from Ahrens, et al., Figure 5 (Ahrens 75), show clustered E1 strength in this region which complicates resolution of other strength which may be present. Subtraction of the E1 strength in this region, visible in Figure 5, from our data indicates E2 strength which exhausts 7% of the E2 isoscalar EWSR in the region 14 to 16 MeV mentioned above (Figure 10).

The states from 7 to 15 MeV together exhaust 23% of the E2 isoscalar EWSR. Adding the contribution of the first excited state at 1.78 MeV, which exhausts 10% of the E2 isoscalar EWSR (EndtL 73), it can be seen that 33% of the isoscalar E2 strength is located in states lying below the GQR region. This is in good agreement with  $(\alpha, \gamma_0)$



results given by Hanna (Han 77) and comparable to results in  $^{24}\text{Mg}$  (YouR 77) and  $^{20}\text{Ne}$  (SzaI 78).

B. The  $(e,e')$  data from 12 to 50 MeV were fit using the line shape fit program solely to establish a credible background. Our reasoning is that using the very restricted background described in IV.B. and forcing it to describe the line at 13 MeV which had a width equal to that of the elastic peak and also the El cross section at 50 MeV, known from  $(\gamma,\text{abs})$  measurements, an acceptable background could be established. As in heavier nuclei the radiation tail alone does not satisfactorily describe the background beyond 20 MeV. The fitted data, after the background subtraction, were analyzed by averaging into  $\sim 1$  MeV wide energy bins compatible with similarly averaged total photon absorption data (Figure 5) converted to equivalent  $(e,e')$  cross sections. The El cross sections thus established were subtracted from the  $(e,e')$  data and the results are shown graphically in Figures 14 to 18. The negative values shown in the  $75^\circ$  spectrum can be attributed to background subtraction from the  $(e,e')$  data. Estimated background subtraction error contributes nearly the total error indicated in the plotted data for the  $60^\circ$  and  $75^\circ$  spectra.

The disentanglement of the El and  $E\lambda$  ( $\lambda > 1$ ) transition strength in the region 12 to 30 MeV is evident in our graphical analysis. The separation of the  $E\lambda$  ( $\lambda > 1$ ) strength into two regions is observed, with a clustering of strength



at 17.5 MeV and a distinct rise in strength which begins at ~20 MeV. This splitting is similar in form to that observed by Youngblood, et al., in  $^{24}\text{Mg}$ . Our analysis shows the state at 17.5 MeV to be E2 in character and to exhaust 22% of the E2 isoscalar EWSR (Figure 12). The contributions to E2 transition strength from the state(s) at 15 MeV and the 17.5 MeV region exhaust 27% of the isoscalar E2 EWSR. This is in general agreement with other results which see from 25 to 40% of the E2 isoscalar E2 strength in the region ~15 to 25 MeV (YouR 77, VanH 77) and with the results of Knöpfle, et al., (KnöW 76) which show 30% of the E2 isoscalar strength in a GQR centered at 19.1 MeV with halfwidth of 5.1 MeV. There is clearly a difference in centroid position for the lower part of the E2 strength, 17.5 MeV compared to the ~19 MeV from  $(\alpha, \alpha')$  (YouR 77, KnöW 76). As in heavier nuclei this difference might be either due to the excitation of the isoscalar monopole resonance (Young 77), or might be an indication that  $(\alpha, \alpha')$  scattering is not that insensitive to the excitation of the isovector dipole resonance as generally believed.

The distinct rise in  $E\lambda$  ( $\lambda > 1$ ) strength at ~20 MeV is observable in all 5 of our spectra. Comparison of this region with the  $(\alpha, \alpha')$  results given by Youngblood, et al., would indicate that this strength is most probably E2 isovector. However, the strength and distribution given by Youngblood, et al., depends on the background assumed. If



one assumes the peak shown in Figure 1c of reference (YouR 77) centered at 27 MeV to be of E2 character as well, 30 to 40% EWSR ( $\Delta T = 0$ ) may be estimated from their data. Unfortunately no complete set of measurements was taken in their experiment for  $^{28}\text{Si}$ , so that no conclusive statement can be drawn.

The presence of transition strength in the region 20 to 30 MeV with  $\lambda > 2$  has been observed by Van der Borg, et al., (VanH 77) and cannot be ruled out in our results. Assuming that the total strength with  $\lambda > 1$  in the region 20 to 30 MeV indicated in our results is E2, it exhausts 65% of the E2 isovector EWSR (Figure 13). This should be considered an upper limit for E2 strength. There may be some isoscalar strength in the 20 to 30 MeV region, but comparison with  $(\alpha, \alpha')$  scattering (YouR 77, KnöW 76) as mentioned above is not decisive. In addition, some of the strength might be monopole strength, but this question can not be solved by our measurement.

A subtraction of a maximum background can be applied to our data as shown by the dashed line in the representative spectrum in Figure 19. This procedure was used in view of the fact that the general form of the background is described quite well by the calculated radiation tail, but that in our form of analysis one has the problem of determining its absolute height. Analysis of the data represented in Figures 14 to 18 after application of this procedure shows E2 strength from 15 to 20 MeV and from 20 to 30 MeV which



exhaust 10 and 20% of the E2 isoscalar/isovector EWSR respectively. These should be considered minimum values for E2 strength in these regions.

The separation of E2 strength in our results might also be considered in conjunction with assumed coexistence of oblate and prolate deformation in  $^{28}\text{Si}$ . Sandorfi, et al., have interpreted a feature in their electrofission results on  $^{28}\text{Si}$  at 28.3 MeV as a resonance or cluster of resonances of E2 character associated with the prolate well of the nucleus (Sand 77). If the state at 17.5 MeV is associated with the ground state oblate well, then the strength associated with the prolate well would be at 24.2 MeV. The existence of a distinct "prolate" E2 branch is not incompatible with our results because we see consistently in all of our spectra after subtraction of the E1 cross section a relative maximum at 24 MeV (Figures 14-18). The separation between the oblate and prolate wells is 6.7 MeV, as inferred from the position of the second  $0^+$  state in  $^{28}\text{Si}$  (DasGH 67).

The observed separation of the continuum E2 strength into two distinct regions, 15 to 20 MeV and 20 to 30 MeV, is in agreement with the result by Szalata, et al. (SzaI 78) for  $^{20}\text{Ne}$ . From this agreement for the two nuclei, of which  $^{20}\text{Ne}$  is prolate and  $^{28}\text{Si}$  is predominantly oblate, one may suspect that the influence of the deformation on the spreading of the transition strength is not as dominant as found recently by Abgrall, et al. (Abg 77).



The data from 30 to 50 MeV was structureless in form and could not be resolved as to multipolarity. Assuming that the cross section in this region is entirely E2, it exhausts 35% of the total EWSR. This should be considered an upper limit. Assuming that the transition strength in this region includes 75% of the isoscalar E3 strength (Ham 72), the remaining strength exhausts 25% of the total E2 EWSR. This is an estimated lower limit for the E2 strength in the region 30 to 50 MeV. A summary of the distribution of E2 strength is shown in Table IV.

It is noted that the  $(\gamma, \text{abs})$  cross section (Figure 5) which was subtracted from our data to get the E2 (and E3) cross section contains some E2 strength, but the magnitude of this strength below 30 MeV is small compared to the error of our measurement and the  $\gamma$ -E1 cross section since the E2 contribution is proportional to  $E_x^3$  (GorP 77).

The  $(\gamma, \text{abs})$  data of the Mainz group (Ahrens 75) have found much publicity recently because they showed clearly that not only the classical Thomas-Reiche-Kuhn (TRK) E1 sum rule to be exhausted at 35 MeV, but furthermore that the cross section corresponding to integration up to pion threshold,  $\sigma(140)$ , is twice the classical sum rule. It is interesting to estimate how much of this strength is due to E2. For this purpose we assume the minimum E2 strengths, which we think are the more reliable values, from Table IV and decide on the missing 40% EWSR on the basis of  $^{27}\text{Al}(\gamma, \text{abs})$



measurements. The  $^{28}\text{Si}$  measurements by Ahrens, et al., have been hampered by coherent pair production above 30 MeV because a silicon monocrystal was used giving rise to the Überall effect (Übe 56).  $^{27}\text{Al}$  should be very similar to  $^{28}\text{Si}$  above 30 MeV and in fact agrees very well with earlier published  $^{28}\text{Si}$  data (Ahrens 72) insofar as both measurements show distinctive cross section at 50-70 MeV. While the observed E2 strength below 20 MeV (30% E2 EWSR) contributes only approximately 5% to the E1 sum rule, this value rises to 20% TRK for the 20% E2 EWSR between 30 and 50 MeV. If we assume the missing 45% of the E2 sum rule to be at 60 MeV, the strength would make a contribution to the integrated  $(\gamma, \text{abs})$  cross section between 10 and 140 MeV equivalent to 30% of the TRK E1 sum rule. It thus seems possible that a major fraction (50%) of the excess strength seen in  $(\gamma, \text{abs})$  is due to E2 strength. The E3 strength, in contrast, would even under the most favorable circumstances (all E3 strength localized at 60 MeV) contribute no more than a few percent.



## VI. CONCLUSIONS

Our results indicate that 35% of the isoscalar E2 strength is exhausted in states below the GQR region. Significant E2 strength is present in a cluster centered around 17.5 MeV which exhausts 22% of the E2 isoscalar EWSR. This relatively small concentration of the E2 strength in the GQR region as compared with heavier nuclei ( $A > \sim 90$ ) is attributable in part to the fragmentation of a significant portion of the E2 strength into the lower lying states.

The E1 strength is concentrated in the region 17 to 22 MeV, but it can be seen from photon absorption data that a significant portion of the total cross section from 20 to 30 MeV is E1 in character. Our analysis shows that the remaining cross section in this region is predominately E2 in character and exhausts 65% of the E2 isovector EWSR.

In our higher momentum transfer ( $\theta = 90, 105, 120$  deg.) spectra significant cross section is apparent in the region 30 to 50 MeV. This cross section exhausts between 25 and 35% of the total E2 EWSR.



TABLE I.

EXPERIMENTAL PARAMETERS INELASTIC  
ELECTRON SCATTERING FROM  $^{28}\text{Si}$

SPECTROMETER ANGLE (DEGREE)	MACHINE ENERGY (MEV)	ELASTIC ENERGY (MEV)	SCHWINGER CORRECTION (EL)
60	91.548	91.100	1.1603
75	91.673	91.121	1.1672
90	91.732	91.060	1.1656
105	92.627	91.213	1.1727
120	92.238	91.257	1.1706

BREMSTRALLUNG CORRECTION (EL)	EFFECTIVE TARGET THICKNESS (G/CM <sup>2</sup> )	RECOIL (EL)	ELASTIC PEAK HALFWIDTH (FWHM) (MEV)
1.1059	0.3614	1.0017405	0.535
1.1161	0.3945	1.0025806	0.538
1.1270	0.4426	1.00348	0.612
1.1510	0.5142	1.0043879	0.582
1.1825	0.626	1.0052319	0.638

ELASTIC MOMENTUM TRANSFER Q (FM)	ELASTIC MOMENTUM TRANSFER SQUARED Q <sup>2</sup> (FM <sup>2</sup> )
0.464	0.215
0.565	0.319
0.656	0.431
0.738	0.545
0.808	0.652

\*\*\* Target thickness 313 (MG/CM<sup>2</sup>) for all runs.



TABLE II.

PARAMETERS FOR CONVERSION OF PHOTON  
ABSORPTION CROSS SECTION TO EQUIVALENT  
ELECTRON SCATTERING CROSS SECTION

THETA	P (1) *	P (2) *	P (3) *	CORR. COEFF.
60	$3.109 \times 10^{-9}$	$-2.820 \times 10^{-12}$	$-7.769 \times 10^{-13}$	0.999
75	$1.239 \times 10^{-9}$	$5.095 \times 10^{-12}$	$-3.462 \times 10^{-13}$	0.999
90	$4.944 \times 10^{-10}$	$4.962 \times 10^{-12}$	$-1.528 \times 10^{-13}$	0.997
105	$1.940 \times 10^{-10}$	$3.102 \times 10^{-12}$	$-6.079 \times 10^{-14}$	0.990
120	$7.415 \times 10^{-11}$	$1.650 \times 10^{-12}$	$-2.243 \times 10^{-14}$	0.996

\* To yield the correct cross section the parameters  
have to be multiplied by  $(\hbar c)^2$



TABLE III.  
SUMMARY OF RESULTS, 4 TO 15 MeV

$E_x$ (MeV)	$\lambda$	$B(\text{fm}^{2\lambda})$	% Isoscalar EWSR
5.1	2	26.8	2.4
7.0	3	5992	22.0
9.9	2	20.2	3.5
11.2	2	18.8	3.7
13.0	2	28.9	6.6
15.0 <sup>*</sup>	2	26.6	7.0

\* E1 strength subtracted.



TABLE IV.  
DISTRIBUTION OF E2 STRENGTH 0 TO 50 MeV

$E_x$ (MeV)	% TOTAL E2 EWSR	
	Maximum	Minimum
0 - 15	15	-- (15)
15 - 20	11*	5
20 - 30	32	10
30 - 50	35	25**
Total:	93	55

\* Includes 3.5% total EWSR centered at 15 MeV.

\*\* Assumes 35% of total E3 strength in the region 30 to 50 MeV (see Hamamoto 1972).



TABLE V.

CONTRIBUTION OF E2 STRENGTH to  $\gamma$  CROSS SECTION

$E_x$	$\sigma$ (mb)	$E_x \cdot B(E2)/\text{EWSR}$	$\int \sigma_\gamma(E2) dE/\text{TRK}$
0 - 20	< 1	20	< 1
20 - 30	< 1	10	< 5
30 - 50	4	25	20
50 - 70	5	45*	30

\* missing strength



## FIGURE CAPTIONS

Figure 1. Spectra of 91.2 MeV electrons scattered inelastically from  $^{28}\text{Si}$  at  $105^\circ$  and  $120^\circ$ . The dash-dotted line under the  $120^\circ$  spectrum is drawn only to guide the eye and is not a fitted or estimated background. The dashed lines beyond 22 MeV are extrapolated from  $(\gamma, \text{abs})$  data and indicate the "excess" cross section in the region 22-50 MeV. The peak at 6.9 MeV in the  $120^\circ$  spectrum has been normalized to the count rate of the  $105^\circ$  spectrum. The prominent rise of this peak with increased momentum transfer is indicative of the assignment of E3 multipolarity.

Figure 2. Spectrum of 91.2 MeV electrons scattered inelastically from  $^{28}\text{Si}$  at  $105^\circ$  and  $120^\circ$ . The spectrum is shown with the background subtracted. The resonances used in fitting this spectrum are described in the text. The "ghost peak" located at 92 % of the elastic energy is subtracted from the spectrum. The spectrum was taken and fitted with 10 data points per MeV. For graphical purposes the number of points for the spectrum was reduced



in the continuum range by a factor of 2.

The fitting range was 4 - 51 MeV.

Figure 3. Comparison of DWBA cross sections for E1 to E3 transitions divided by the Mott cross sections. The E1 transition is based on the Myers-Swiatecki model while the E2 and E3 transitions are based on the Goldhaber-Teller model.

Figure 4. Comparison of the experimental form factors of the Goldhaber-Teller, Steinwedel-Jensen, and Myers-Swiatecki models for E1 transition and excitation energy of 0 MeV.

Figure 5. The photon absorption cross section of  $^{28}\text{Si}$ . The data are from Ahrens, et al. (Ahrens 75).

Figure 6. Comparison of the DWBA and experimental form factors for the state at 5.1 MeV, which exhausts 2.4% of the E2 isoscalar EWSR.

Figure 7. Comparison of the DWBA and experimental form factors for the state at 7.0 MeV which exhausts 22% of the E3 isoscalar EWSR.

Figure 8. Comparison of the DWBA and experimental form factors for the state at 9.9 MeV which exhausts 3.5% of the E2 isoscalar EWSR.



Figure 9. Comparison of the DWBA and experimental form factors for the state at 11.2 MeV which exhausts 3.7% of the E2 isoscalar EWSR.

Figure 10. Comparison of the DWBA and experimental form factors for the state at 13.0 MeV which exhausts 6.6% of the E2 isoscalar EWSR.

Figure 11. Comparison of the DWBA and experimental form factors for the state at 15 MeV. The E1 strength represented by the  $(\gamma, \text{abs})$  data in Figure 5 from 14 to 16 MeV has been subtracted from the  $(e, e')$  data and the remaining transition strength form factors plotted.

Figure 12. Comparison of the DWBA and experimental form factors for the region 15 to 20 MeV. The E1 strength represented by the  $(\gamma, \text{abs})$  data of Figure 5 in the same region has been subtracted from the  $(e, e')$  data and the remaining transition strength form factors plotted.

Figure 13. Comparison of the DWBA and experimental form factors for the region 20 to 30 MeV. The E1 strength represented by the  $(\gamma, \text{abs})$  data of Figure 5 in the same region has been subtracted from the  $(e, e')$  data and the remaining transition strength form factors plotted. While the E3 form factor gives a better fit, an E3



assignment would lead to a 200% of the isoscalar sum rule, which is impossible. Since little E3 strength is expected in this region, no attempt was made to subtract E3 strength, which would be arbitrary.

Figure 14. Inelastic cross section at  $60^\circ$ , 12 to 30 MeV. The  $(e,e')$  data have been averaged into 1 MeV energy bins and are represented by the open circles. The  $(\gamma, \text{abs})$  data converted to equivalent  $(e,e')$  cross section were similarly averaged and are represented by the closed circles. The differences  $(e,e')$  minus  $(\gamma, \text{abs})$  (equivalent) is represented by the halfmoon circles.

Figure 15. Same as Figure 14 except for  $75^\circ$ .

Figure 16. Same as Figure 14 except for  $90^\circ$ .

Figure 17. Same as Figure 14 except for  $105^\circ$ .

Figure 18. Same as Figure 14 except for  $120^\circ$ .

Figure 19. Same as Figure 18 showing maximum background as dotted line.



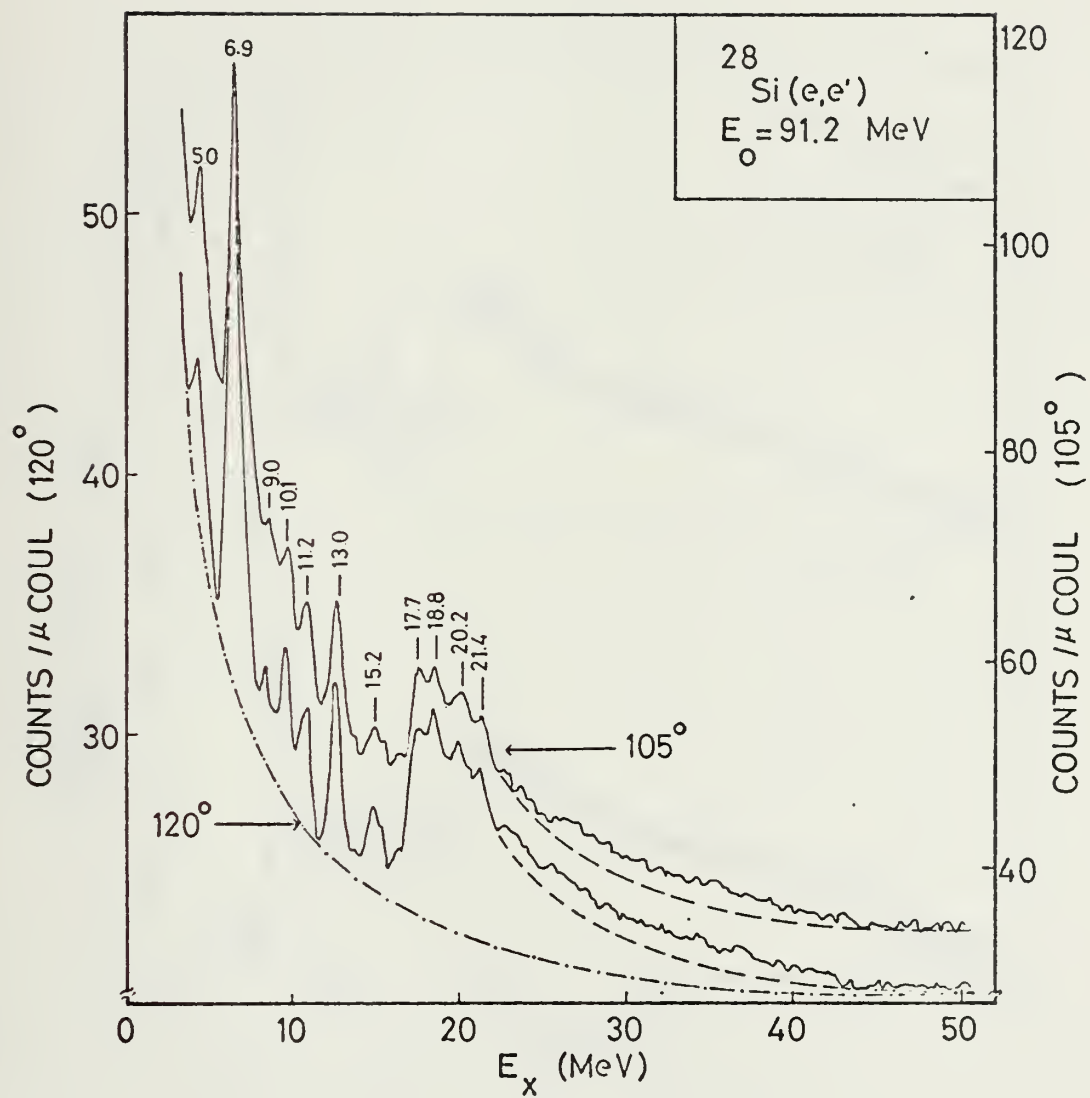


Figure 1. Inelastic spectra at  $105^\circ$  and  $120^\circ$ .



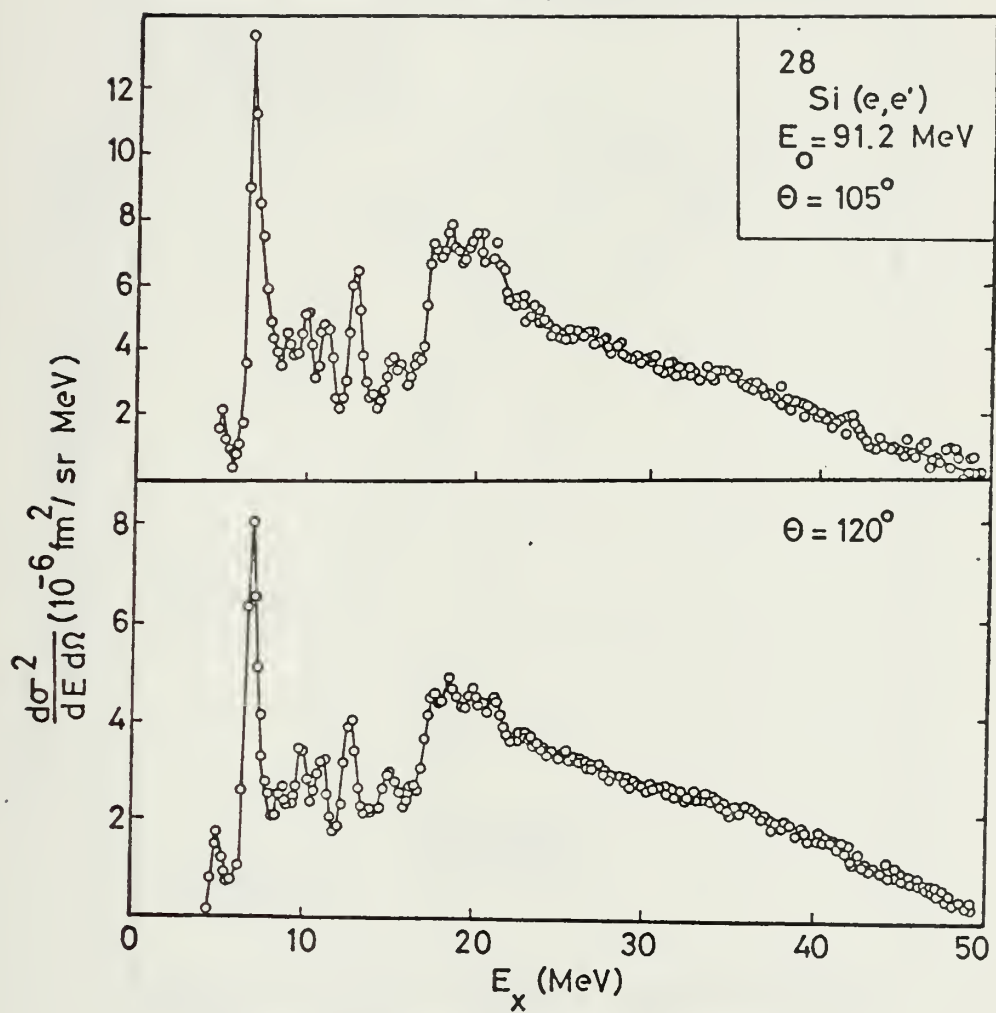


Figure 2. Inelastic spectra at  $105^\circ$  and  $120^\circ$ .



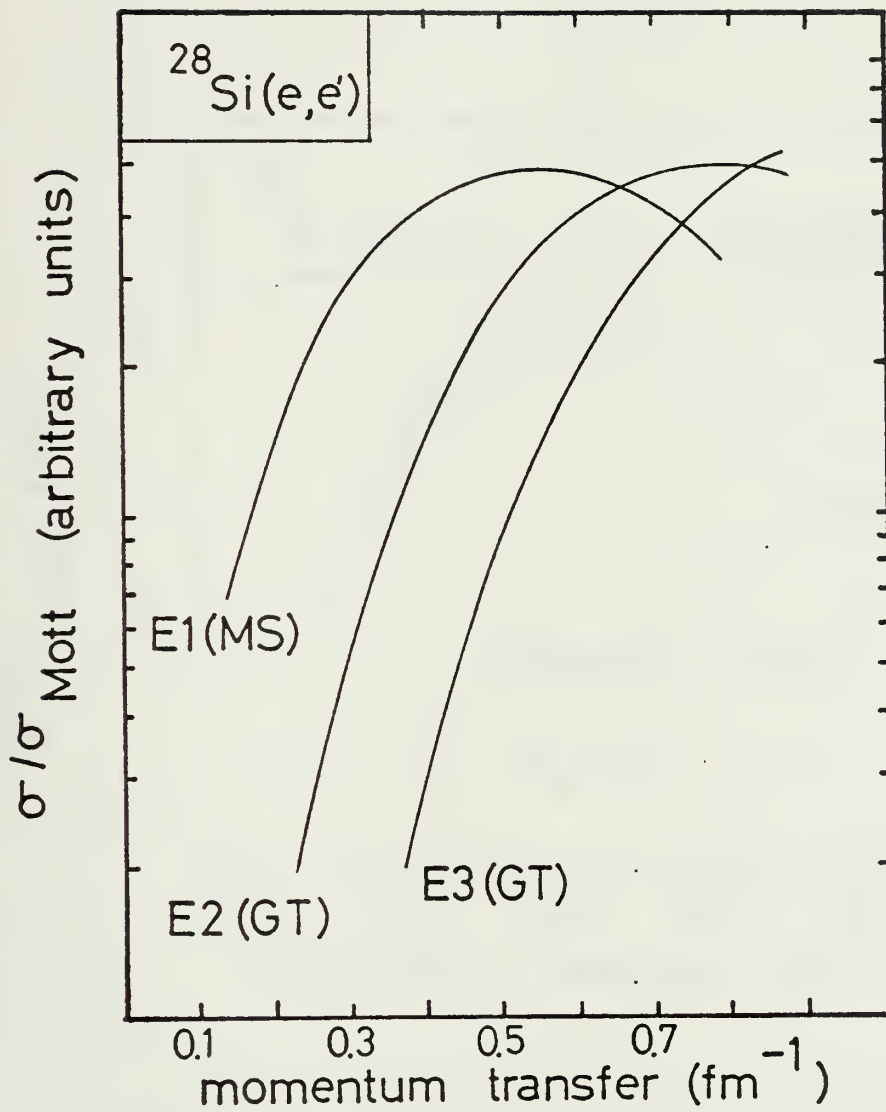


Figure 3. Comparison of DWBA cross sections



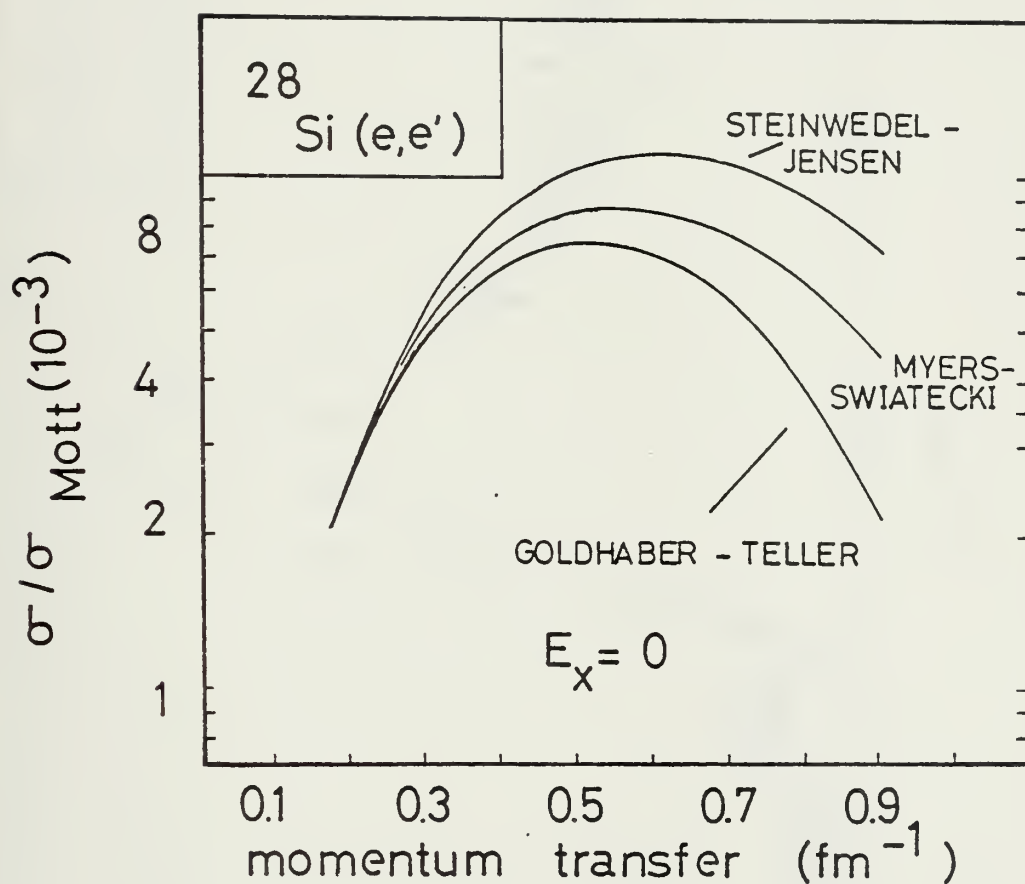


Figure 4. Comparison of Goldhaber-Teller, Steinwedel-Jensen, and Myers-Swiatecki models for DWBA calculations for E1 transitions.



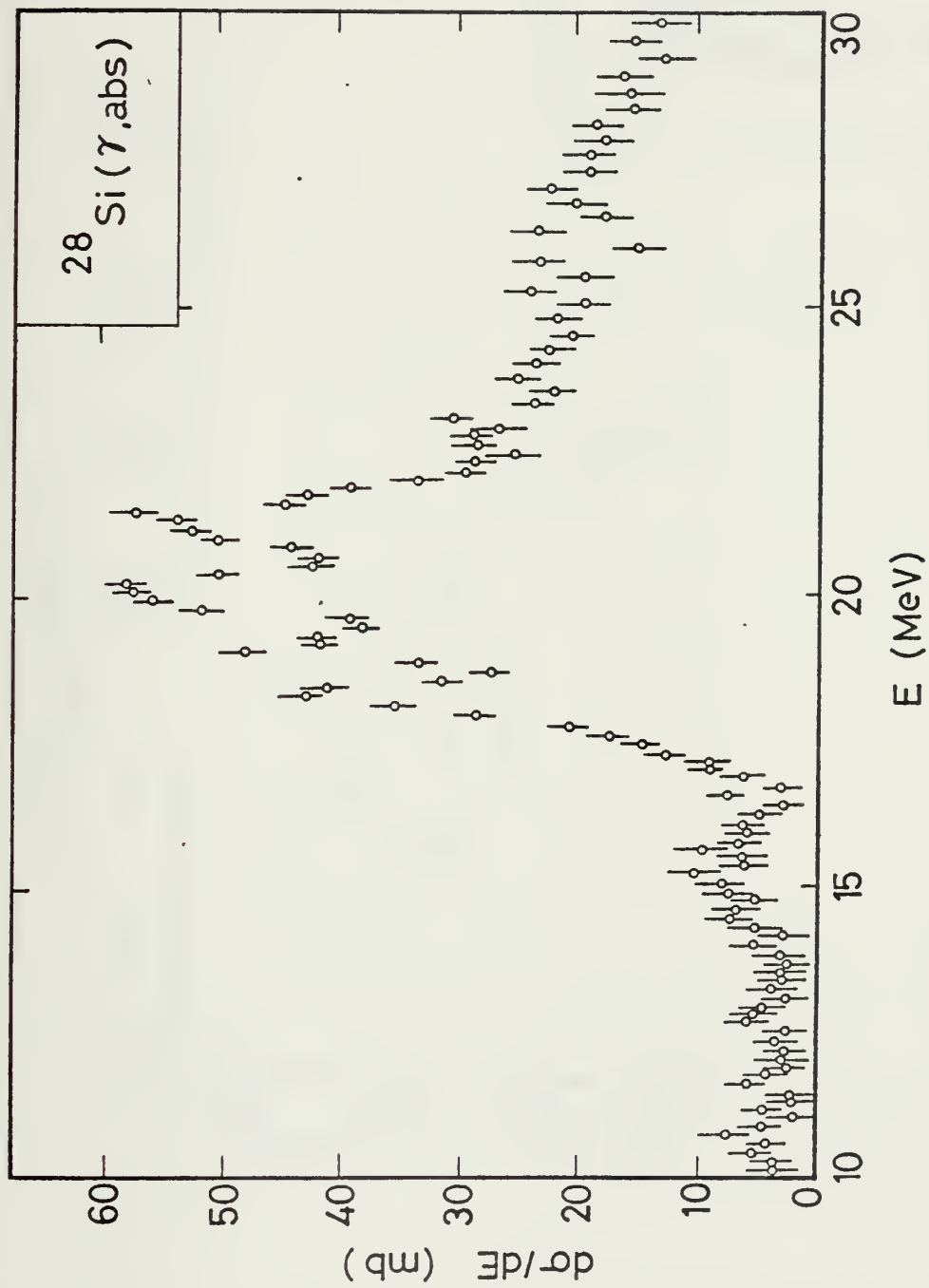


Figure 5. Gamma absorption data from Ahrens, et al. (Ahrens 75).



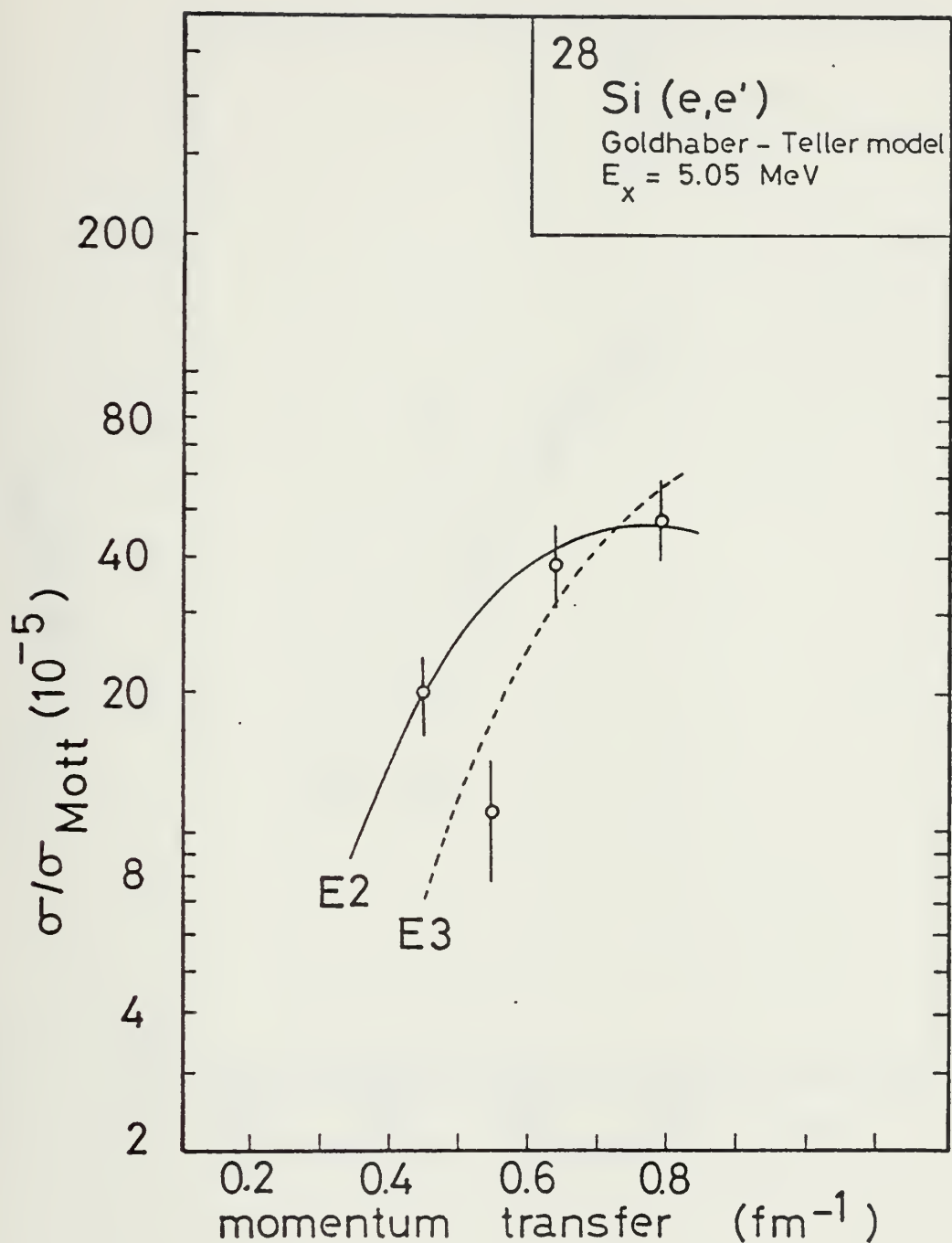


Figure 6. Comparison of the DWBA and experimental form factors for the resonance at 5.1 MeV.



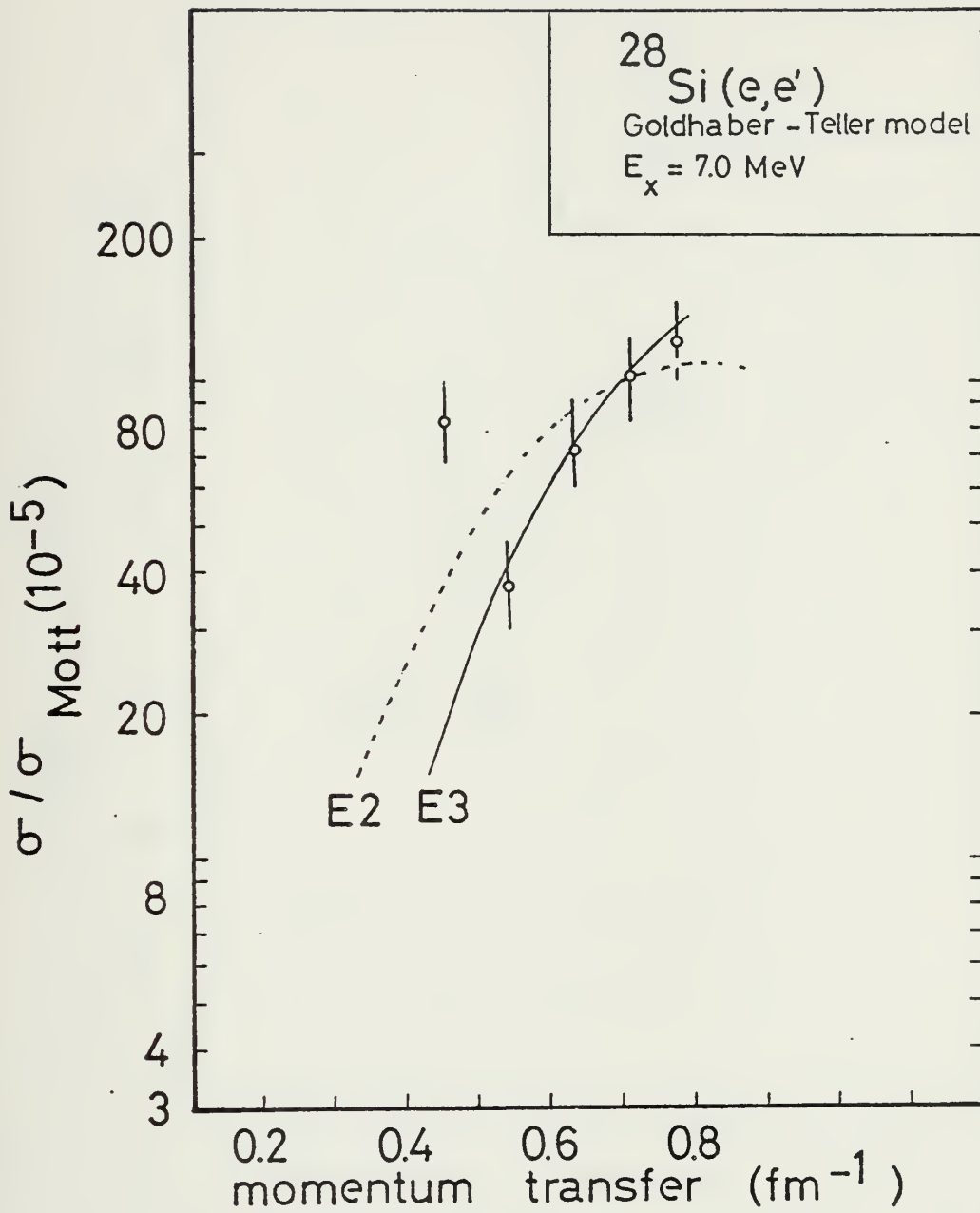


Figure 7. Comparison of the DWBA and experimental form factors for the resonance at 7.0 MeV.



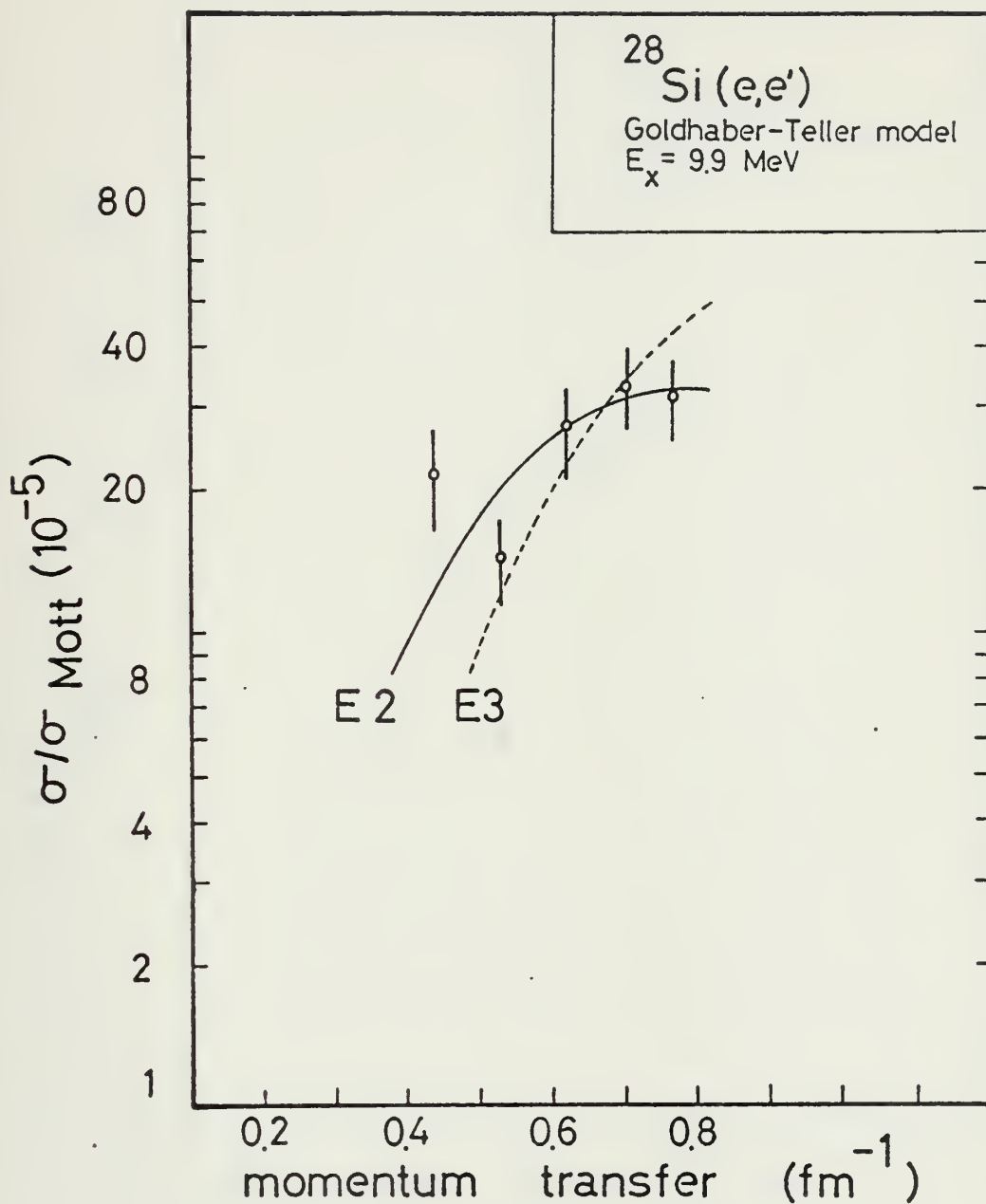


Figure 8. Comparison of the DWBA and experimental form factors for the resonance at 9.9 MeV.



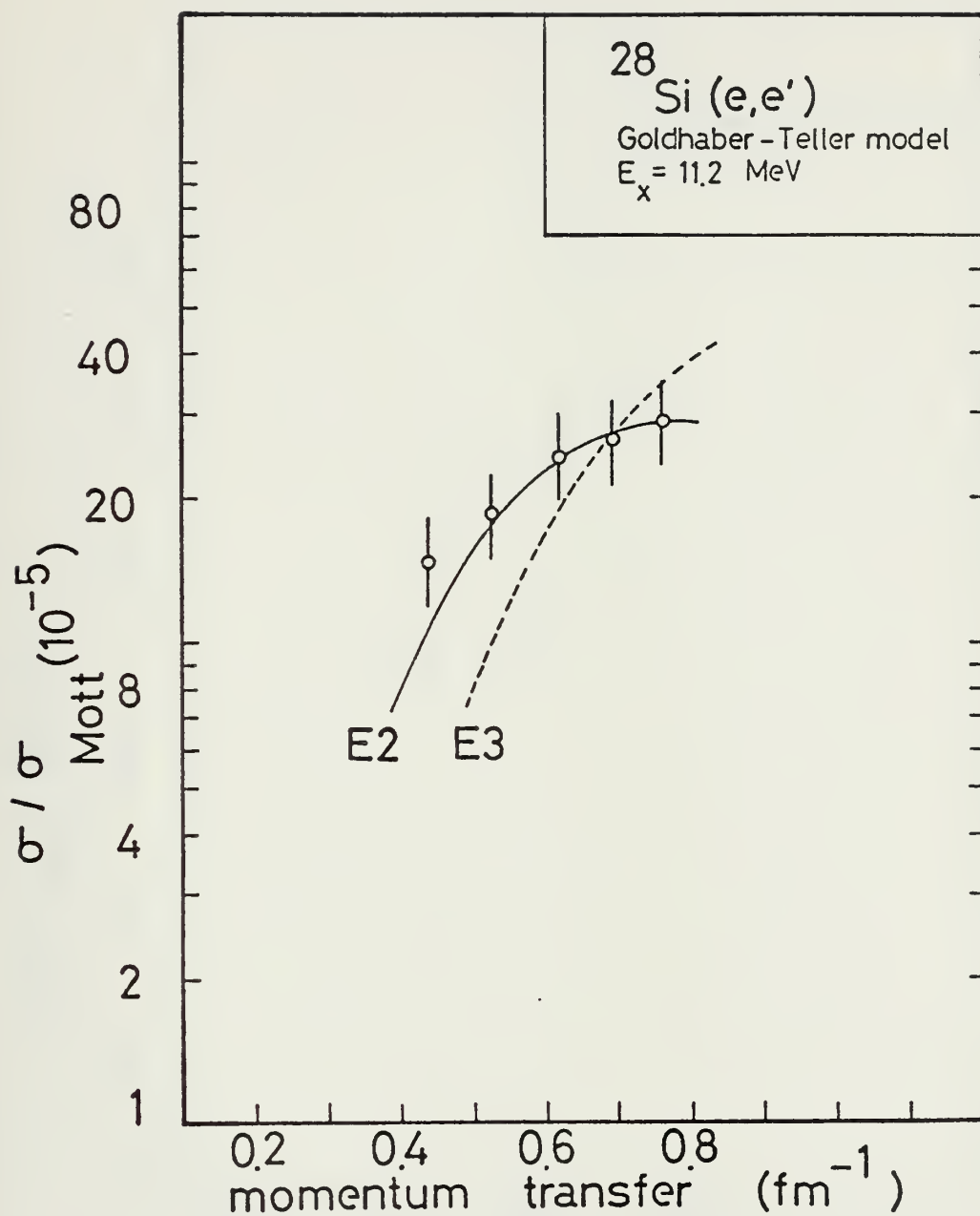


Figure 9. Comparison of the DWBA and experimental form factors for the resonance at 11.2 MeV.



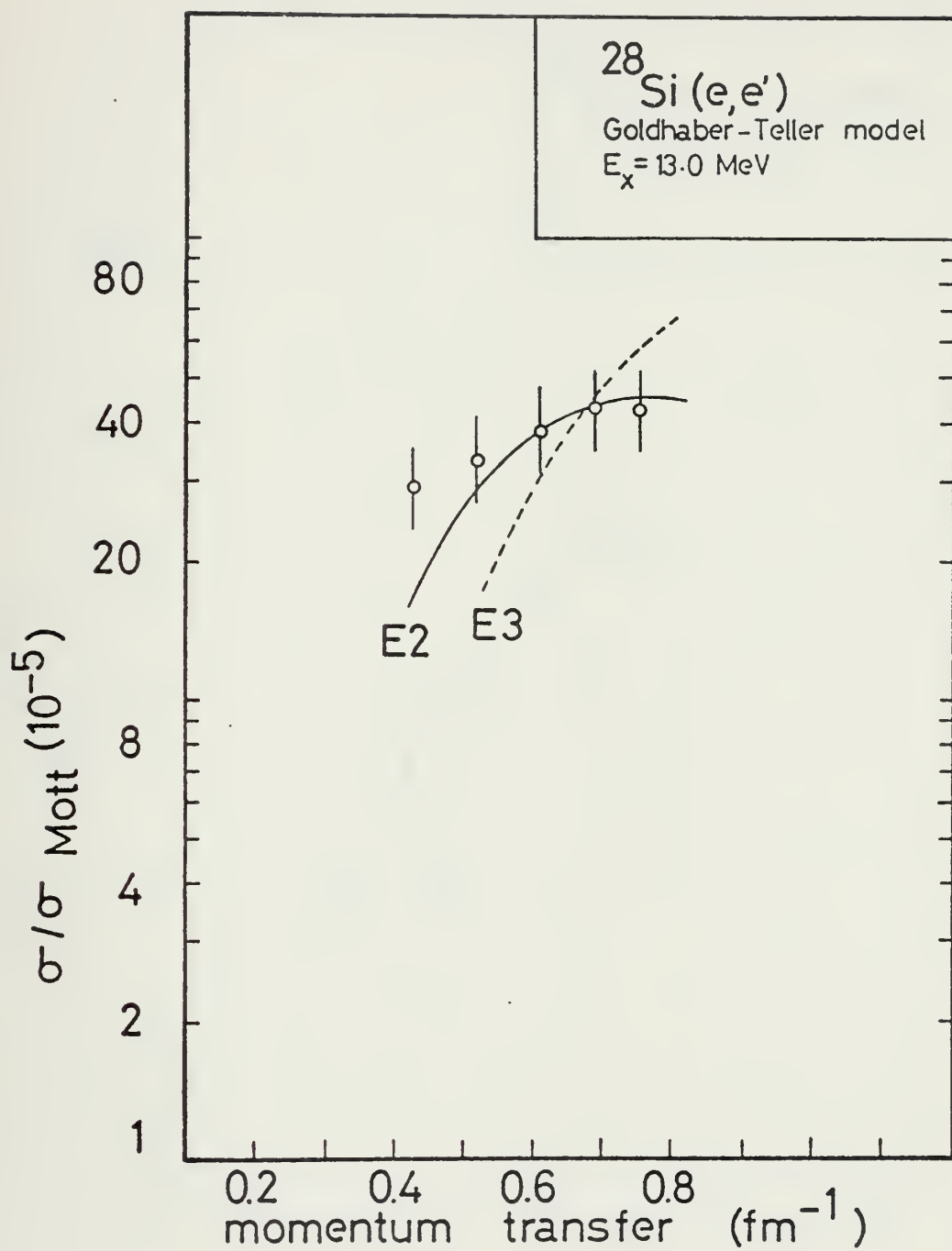


Figure 10. Comparison of the DWBA and experimental form factors for the resonance at 13.0 MeV.



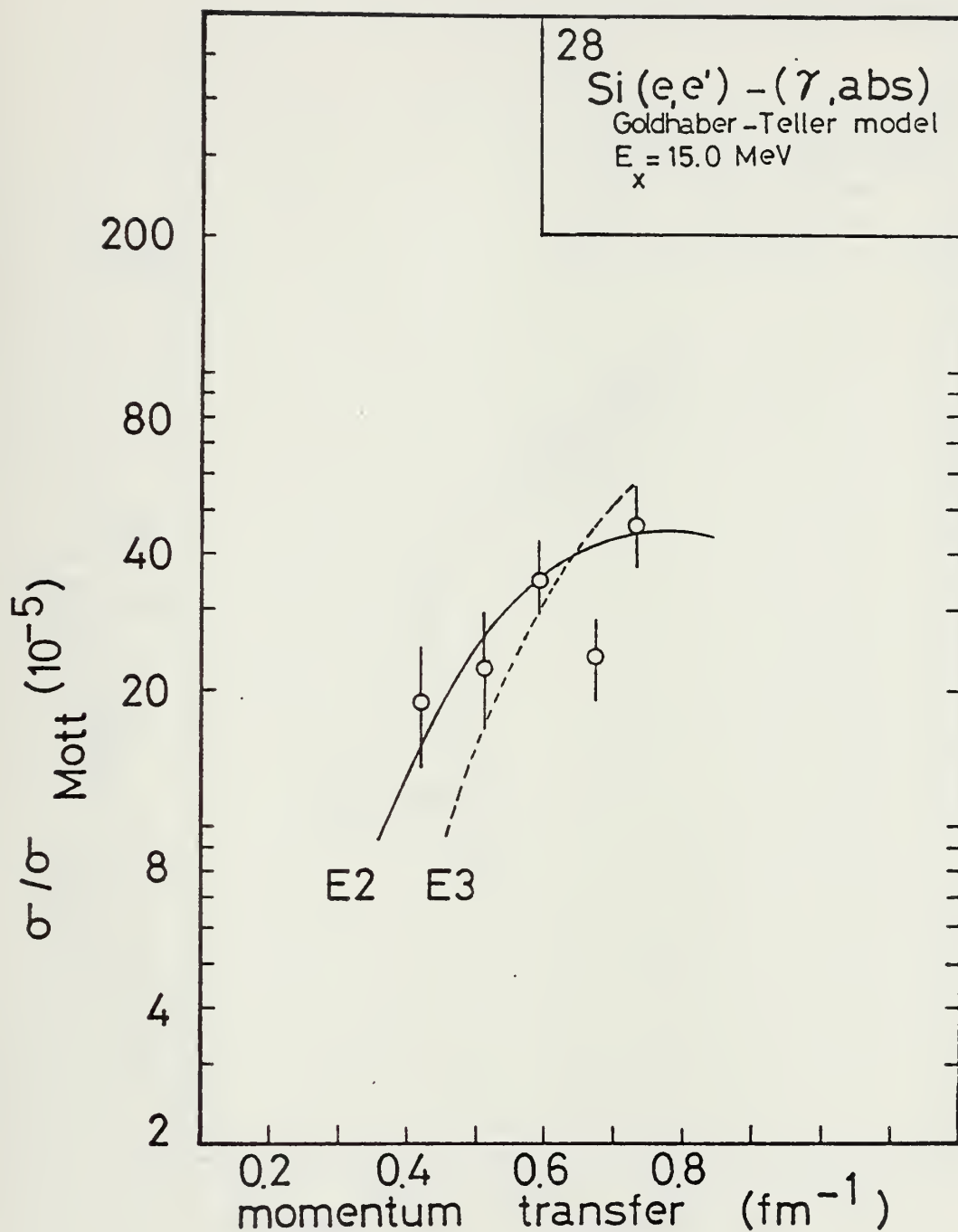


Figure 11. Comparison of the DWBA and experimental form factors for the resonance at 15.0 MeV. The (γ,abs) cross section strength has been subtracted.



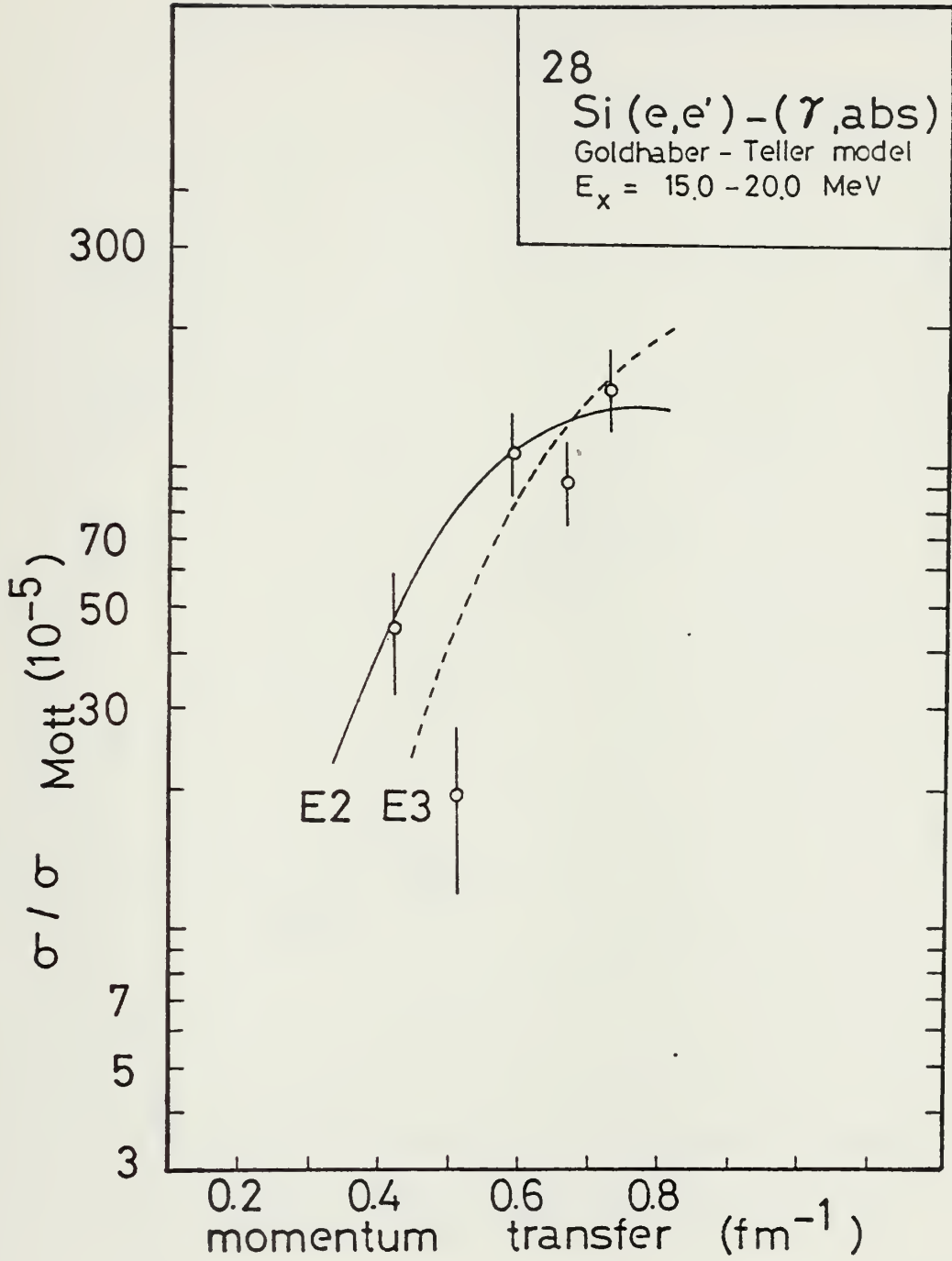


Figure 12. Comparison of the DWBA and experimental form factors for the region 15 to 20 MeV with ( $\gamma$ ,abs) strength subtracted.



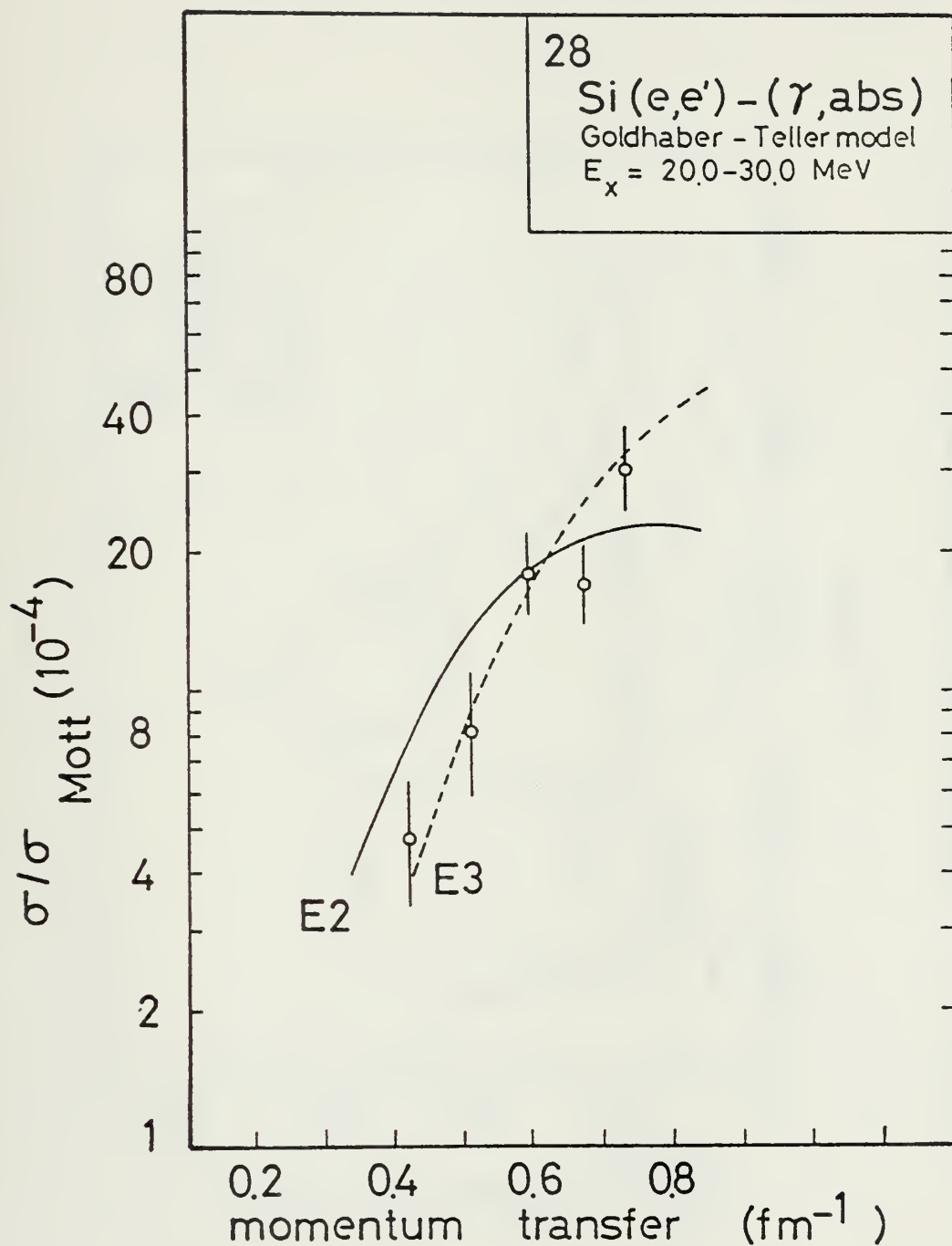


Figure 13. Comparison of the DWBA and experimental form factors for the region 20 to 30 MeV with the ( $\gamma$ ,abs) strength subtracted.



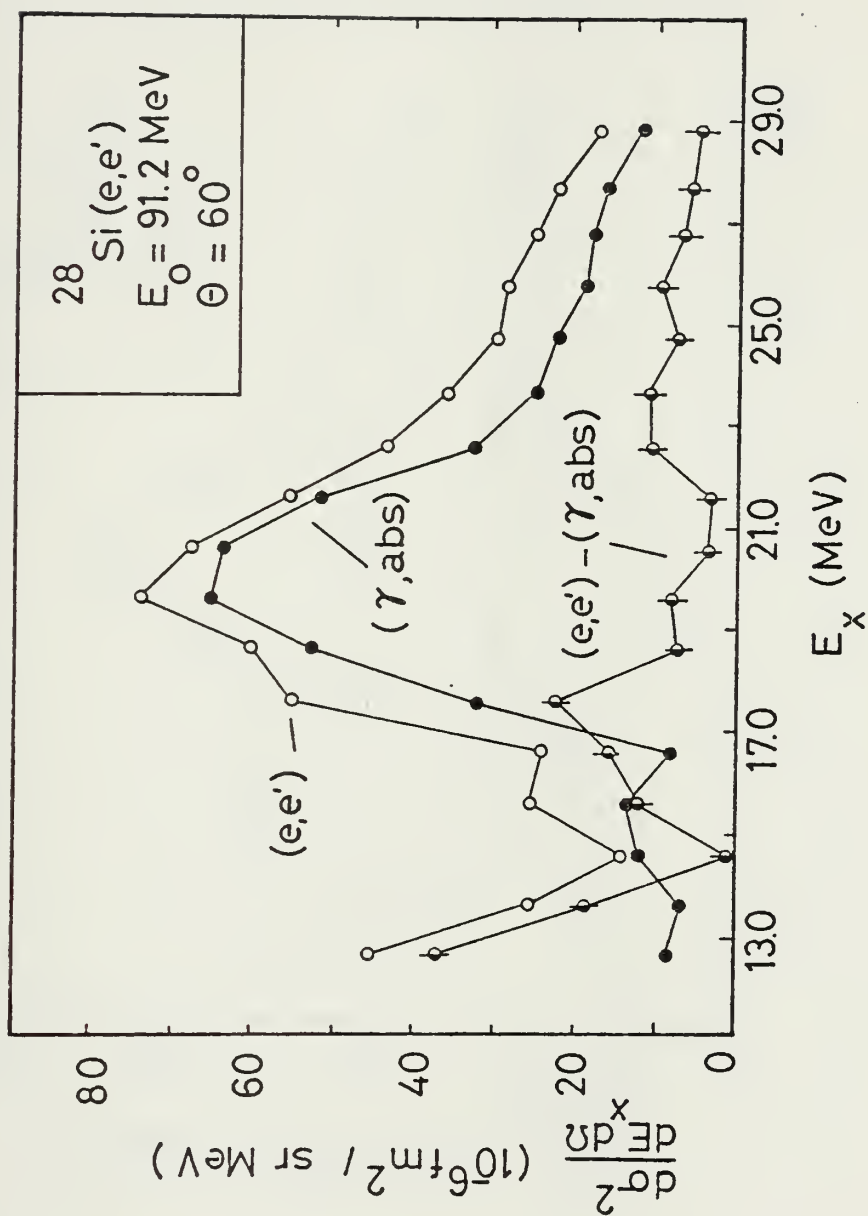


Figure 14. Inelastic cross section at  $60^\circ$ , 12 to 30 MeV, showing the subtraction of  $(\gamma, \text{abs})$  data.



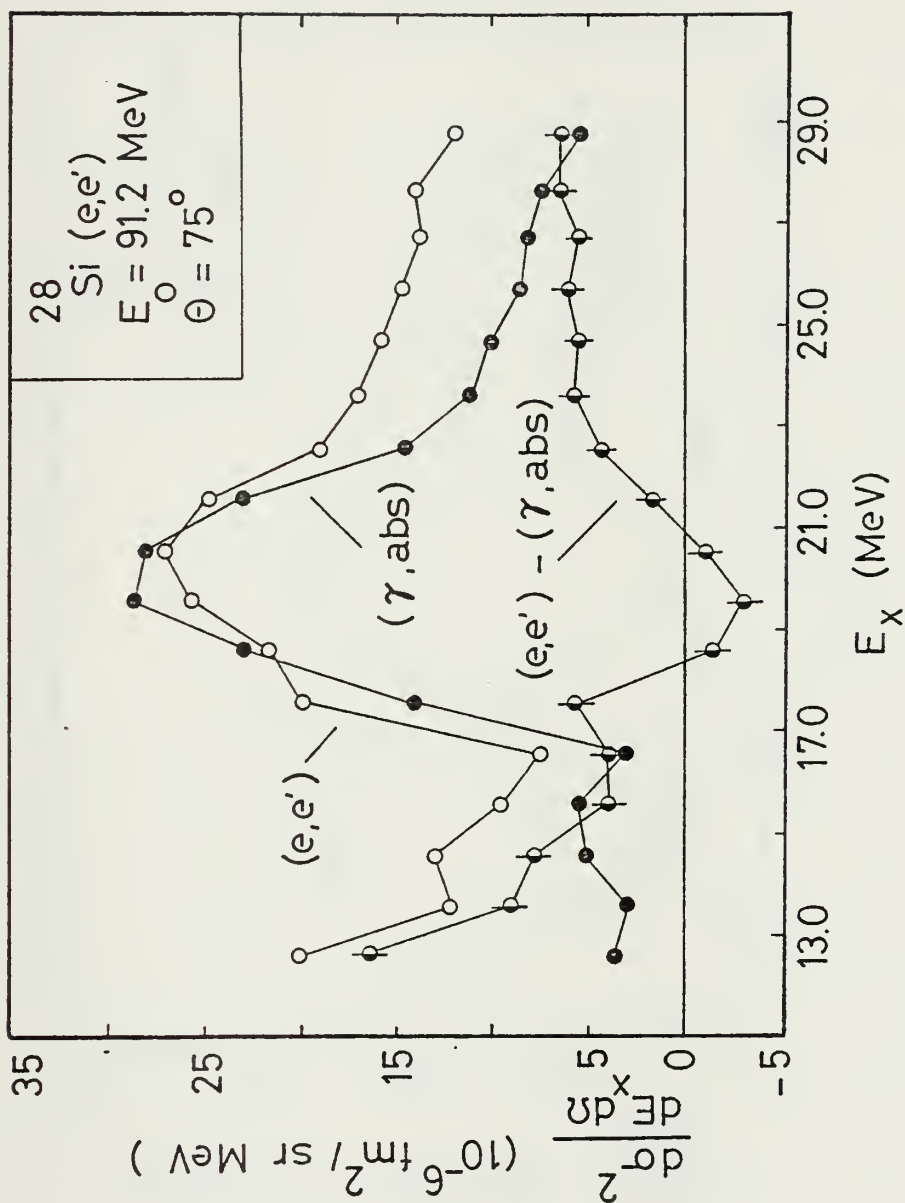


Figure 15. Inelastic cross section at  $75^\circ$ , 12 to 30 MeV, showing the subtraction of  $(\gamma, \text{abs})$  data.



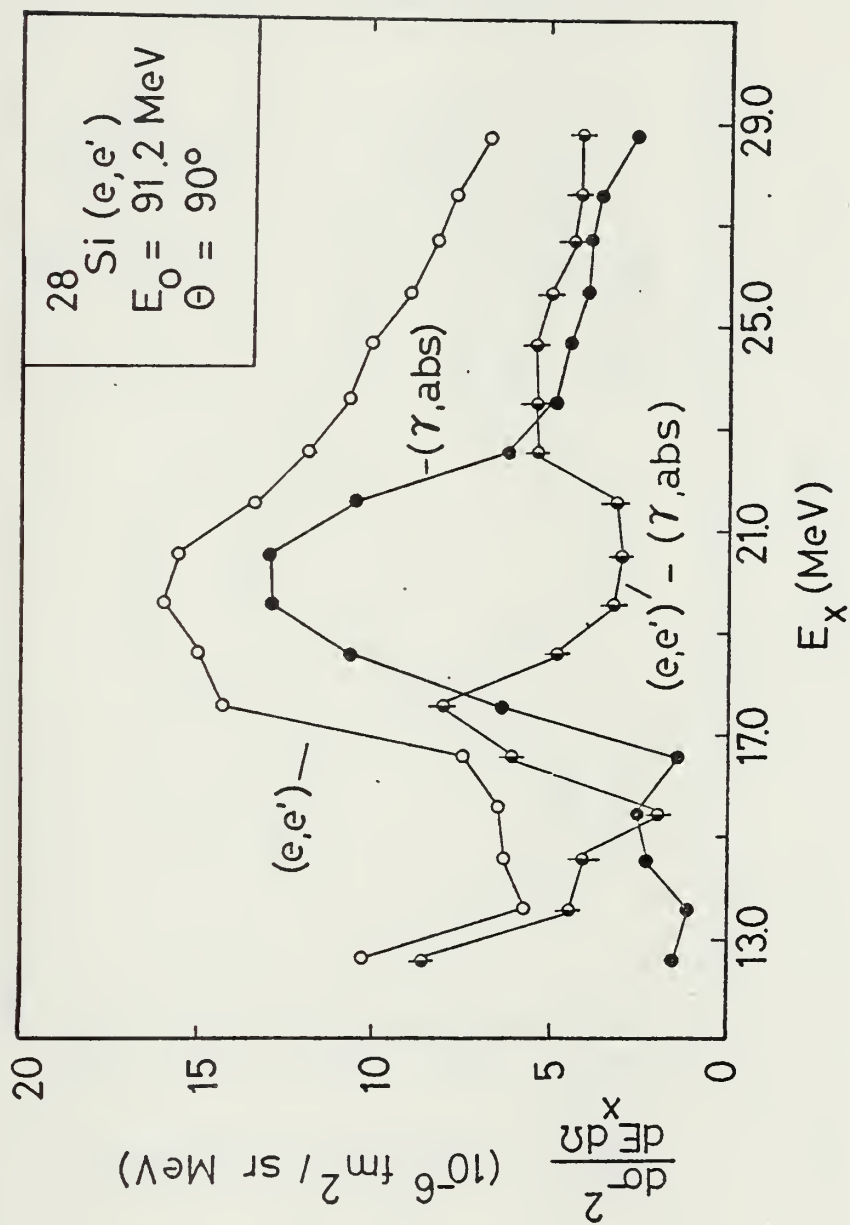


Figure 16. Inelastic cross section at  $90^\circ$ , 12 to 30 MeV, showing the subtraction of  $(\gamma, \text{abs})$  data.



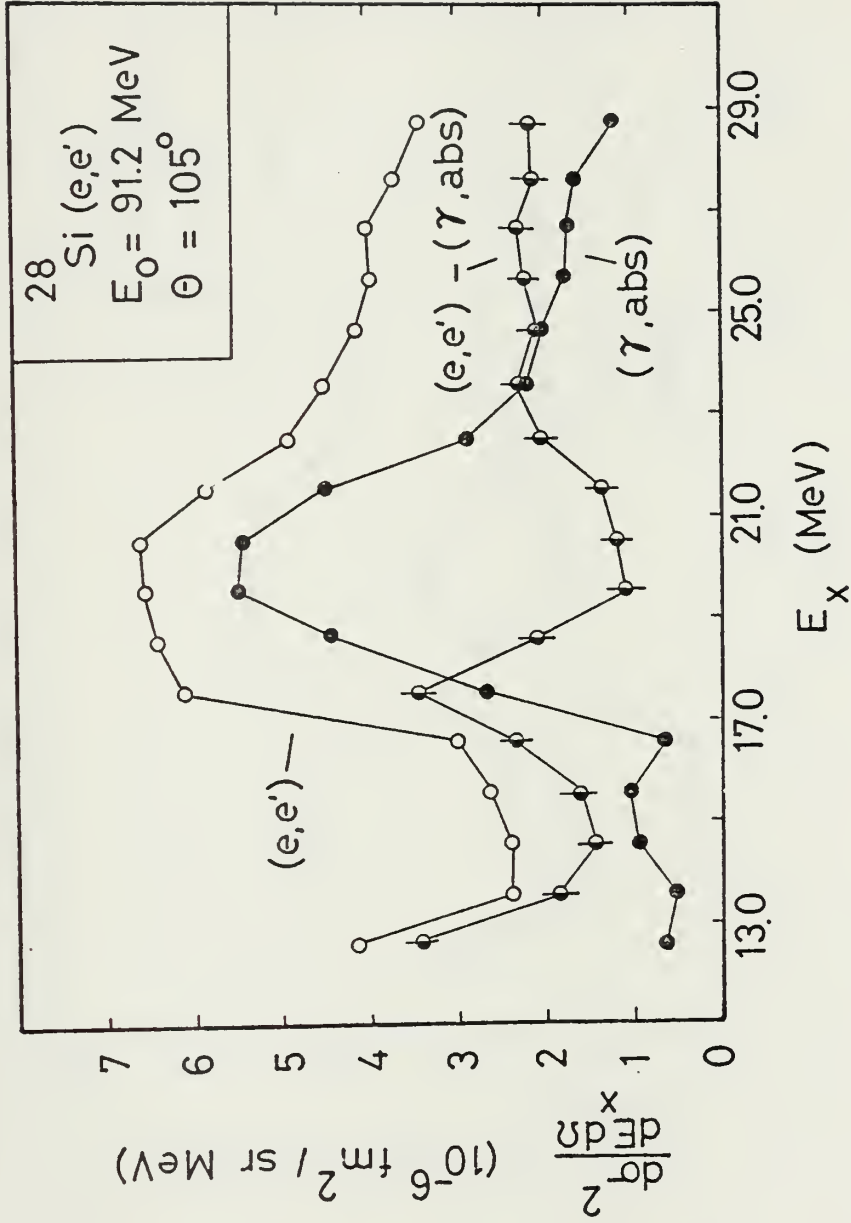


Figure 17. Inelastic cross section at  $105^\circ$ , 12 to 30 MeV, showing the subtraction of  $(\gamma,abs)$  data.



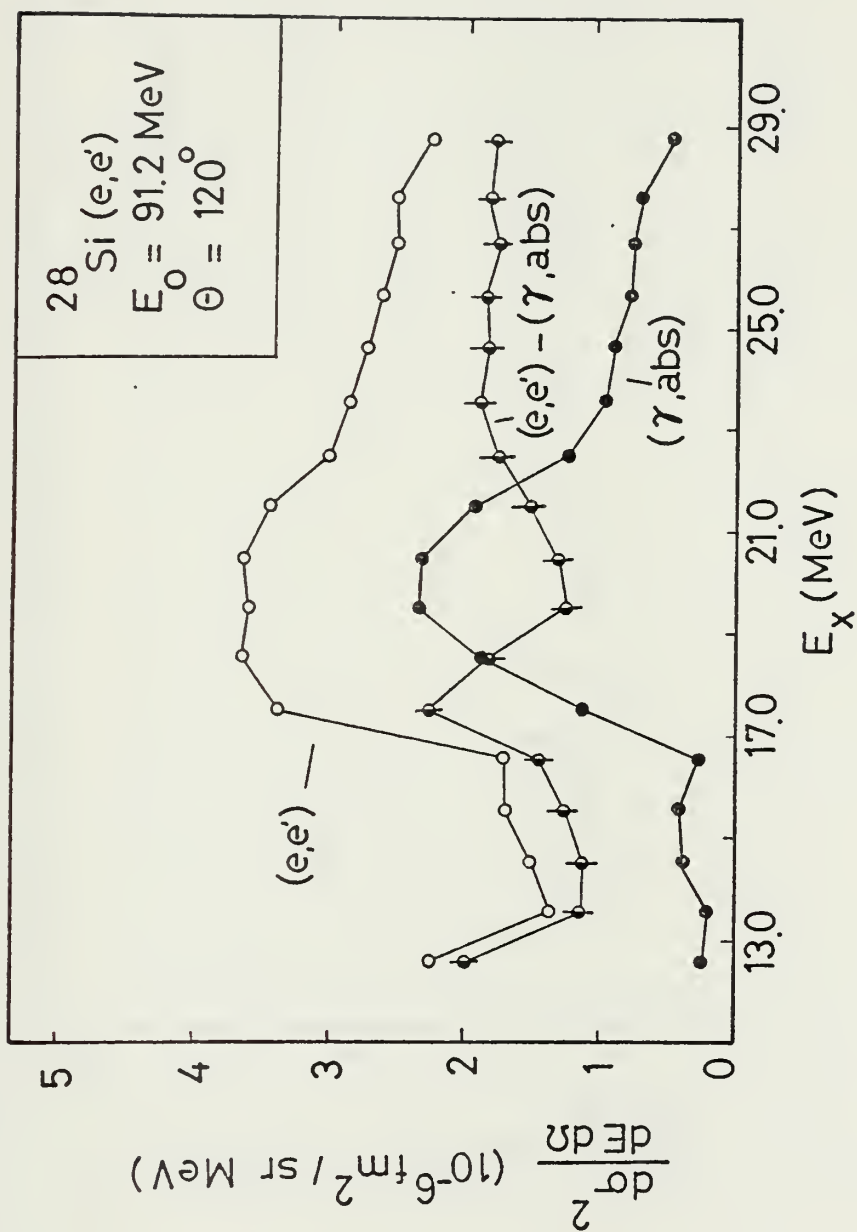


Figure 18. Inelastic cross section at  $120^\circ$ , 12 to 30 MeV, showing the subtraction of  $(\gamma, \text{abs})$  data.



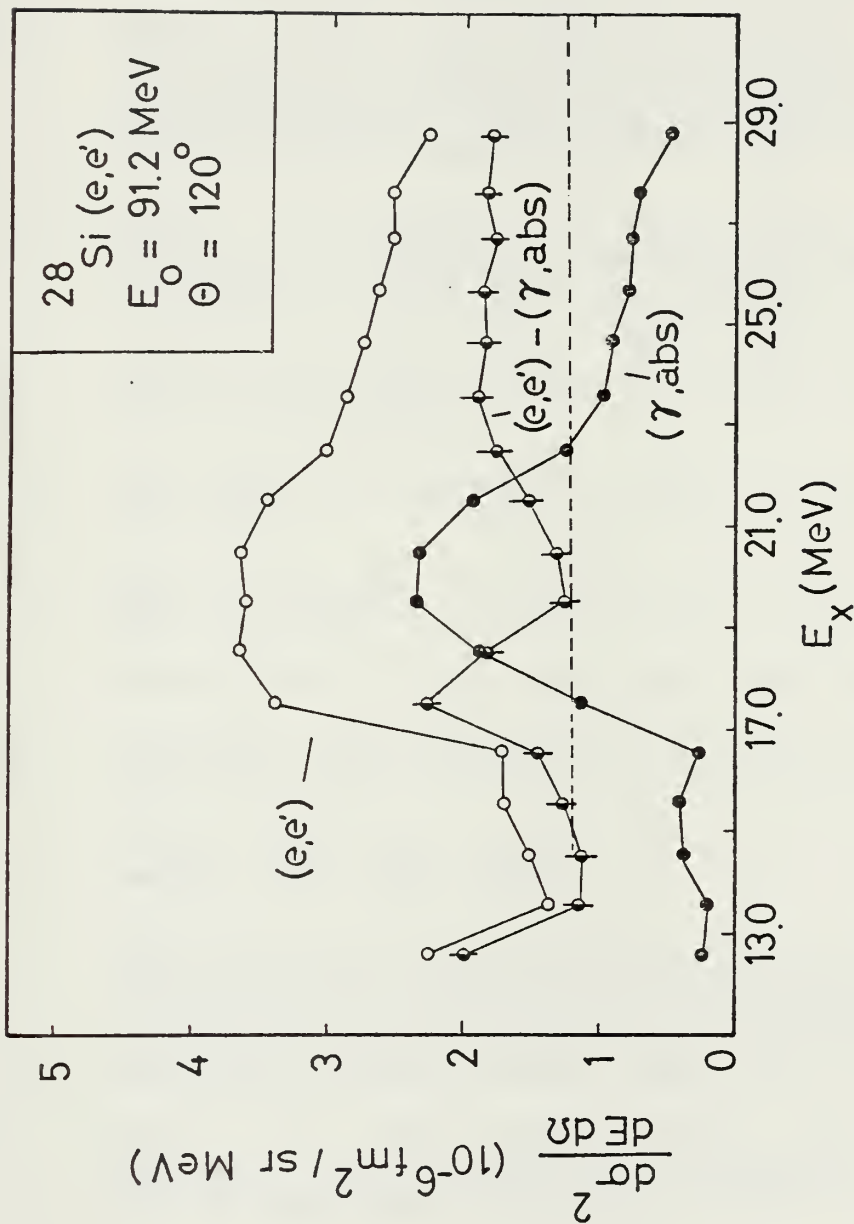


Figure 19. Inelastic cross section at  $120^\circ$ , 12 to 30 MeV, showing the subtraction of  $(\gamma, \text{abs})$  data with maximum background.



## LIST OF REFERENCES

- Abg 77      Abgrall, Y., Morand, B., Caurier, E., and  
Grammaticos, B., Phys. Rev. Lett. 39, 922, 1977.
- Ahrens 72    Ahrens, et al., from "Nuclear Structure Studies  
Using Electron Scattering and Photoreaction,"  
Proceedings of the International Conference on  
Nuclear Structure Using Electron Scattering and  
Photoreaction, Sendai, 1972, p. 213.
- Ahrens 73    Ahrens, J., Borchert, H., Czock, K.H.,  
Eppler, H.B., Gimm, H., Gundrum, H., Kroning,  
M., Riehn, P., Sita Ram, G., Zieger, A., and  
Ziegler, B., Nuc. Phys., A251, 479, 1975.
- BusP76      Buskirk, F.R., and Pitthan, R., Bull. Am. Phys.  
Soc. 21, 683, 1976.
- DasGH 67    Das Gupta, S., Harvey, M., Nucl. Phys. A94,  
602, 1967.
- EndtL 73    Endt, P.M., and van der Leun, C., Nucl. Phys.  
A214, 1, 1973.
- Fer 57      Ferrell, R.A., Phys. Rev. 107, 1631, 1957.
- Golt 48      Goldhaber, M., and Teller, E.: Phys. Rev.,  
74, 1046, 1948.
- GorP 77      Gordon, E.F., and Pitthan, R., Nucl. Instrum.  
Methods, 145, 569, 1977.
- Ham 72      Hamamoto, I., from "Nuclear Structure Studies  
Using Electron Scattering and Photoreaction,"  
Proceedings of the International Conference  
on Nuclear Structure Using Electron Scattering  
and Photoreaction, Sendai, Sept. 1972, p. 203.
- Han 77      Hanna, S.S., "Erice Summer School Photonic  
Lectures," in "Lecture Notes in Physics,"  
Vol. 61 (Springer, Heidelberg 1977).
- KnöW 76    Knöpfle, K.T., Wagner, G.J., Kiss, A., Rogge, M.,  
Mayer-Boricke, C., and Bauer, Th., Phys. Lett.,  
64B, 263, 1976.
- Pit 77      Pitthan, R., Buskirk, F.R., Dally, E.B.,  
Shannon, J.O., Smith, J.H., Phys. Rev., 16,  
970, 1977.



- Pit 73      Pitthan, R., Z. Physik, 260, 283, 1973.
- San 77      Sandorfi, A.M., Kilius, L.R., Lee, H.W., and  
Litherland, A.E., Phys. Rev. Lett, 38, 1463,  
1977.
- SteJ 50      Steinwedel, H. and Jensen, J.H.D., Z. Naturforsch,  
5a, 413, 1950.
- SzaI 78      Szalata, Z.M., Itoh, K., Peterson, G.A., Flanz, J.,  
Fivozinsky, S.P., Kline, F.J., Lightbody, J.W. Jr.,  
Maruyama, X.K., and Penner, S., Phys. Rev. 17,  
435, 1978.
- The 72      Theissen, H.: Springer Tracts in Modern Physics  
Vol. 65, Springer-Verlag, Berlin, 1972.
- TuaW 68      Tuan, S.T., Wright, L.E., Onley, D.S.: Nucl.  
Instr. Meth., 60 70, 1968.
- Übe 56      Überall, Phys. Rev. 103 (1956) 1055.
- Übe 71      Überall, H., Electron Scattering from Complex  
Nuclei, Academic Press, 1971.
- VanH 77      Van der Borg, K., Harakey, M.N., Van de Werf,  
S.Y., Woude, A., Bertrand, F.E., Phys. Lett.,  
67B, 405, 1977.
- WarW 69      Warburton, E.K., and Weneser, J.: The Role of  
Isospin in Electromagnetic Transitions, ed. by  
Wilerson, D.H., North-Holland Publishing Company,  
Amsterdam, 1969.
- Young 77      Youngblood, D.H., Rozsa, C.M., Moss, J.M.,  
Brown, D.R., and Bronson, J.D., Phys. Rev. Lett.  
39 1188, 1977.
- YouR 77      Youngblood, D.H., Rozsa, C.M., Moss, J.M.,  
Brown, D.R., and Bronson, J.D., Phys. Rev. 15,  
1644, 1977.
- ZieP 68      Ziegler, J.F., and Peterson, G.A., Phys. Rev.,  
165, 1337, 1968.



INITIAL DISTRIBUTION LIST

	No. Copies
1. Defense Documentation Center Cameron Station Alexandria, Virginia 22314	2
2. Library, Code 0142 Naval Postgraduate School Monterey, California 93940	2
3. Physics Library, Code 61 Department of Physics and Chemistry Naval Postgraduate School Monterey, California 93940	2
4. Professor F. R. Buskirk, Code 61Bs Department of Physics and Chemistry Naval Postgraduate School Monterey, California 93940	3
5. Professor R. Pitthan, Code 61Pt Department of Physics and Chemistry Naval Postgraduate School Monterey, California 93940	2
6. Professor J.N. Dyer, Code 61Dy Department of Physics and Chemistry Naval Postgraduate School Monterey, California 93940	1
7. LT. Edward Hunter, USN USS Mount Whitney LCC-20 Fleet Post Office New York, New York 09501	1
8. LT. Gregory Pozinsky, USN Class 60 SWOSCOLCOM, Bldg 446 Newport, Rhode Island 02840	1







Thesis  
H949  
c.1

Hunter

Inelastic electron  
scattering in  $^{28}\text{Si}$   
between 4 MeV and 50  
MeV excitation energy.

176779

Thesis  
H949  
c.1

Hunter

Inelastic electron  
scattering in  $^{28}\text{Si}$   
between 4 MeV and 50  
MeV excitation energy.

176779

Inelastic electron scattering in 28 Si b



3 2768 002 13275 5

DUDLEY KNOX LIBRARY